INGV-T3 Research Project 2015-2016

HYPSTHER

HYBRID GROUND MOTION PREDICTION EQUATIONS FOR PSHA PURPOSES: THE STUDY CASE OF SOUTHERN ITALY

Task 4 (WG-T4)

SEISMIC HAZARD ASSESSMENT

Marco Santulin[(1)], Maria D'Amico[(2)], Giovanni Lanzano[(2)]

[(1)] Istituto Nazionale di Geofisica e Vulcanologia, Sezione di Milano, c/o OGS, Trieste, Italy
[(2)] Istituto Nazionale di Geofisica e Vulcanologia, Sezione di Milano, Via Corti 12, 20133 Milano, Italy

Abstract

The aim of the last task of the project was to combine all the products from other tasks and to perform a series of sensitivity studies on models and/or parameters to evaluate their impact on the seismic hazard assessment, according to the approach of the seismotectonic probabilism, originally proposed by Cornell (1968). The final step will be to evaluate the impact of the employment of the hybrid GMPEs in the assessment of the seismic hazard. Some significant test sites in Southern Italy has been selected because of the presence of critical infrastructures (Milazzo ME, Priolo Gargallo SR, Gioia Tauro RC) to test the variability of the results at different return periods, depending on the relevance of the infrastructure studied and corresponding to the Serviceability Limit State for damage control (SLD) and the Ultimate Limit State for collapse prevention (SLC) of the European EC8 (CEN, 2004) and Italian NTC08 (CS.LL.PP., 2008) seismic codes.

Introduction

A probabilistic seismic hazard analysis provides an estimate of the frequency of exceeding specified levels of ground motion at a site by integrating the contributions of earthquakes of all possible magnitudes and locations in a consistent manner. This method has many applications in the field of earthquake engineering, including the design or retrofitting of critical facilities (for example, nuclear reactors, bridges, dams, and hospitals) and the containment of hazardous waste. More recently, seismic hazard analyses have also been used for the determination of earthquake insurance coverage of private homes and businesses.

The seismic hazard obtained following the seismotectonic probabilism approach, as proposed for the first time by Cornell (1968) needs the following input data: the seismic source geometry, the earthquake potential (which is defined in terms of average number of earthquakes per magnitude class, and maximum magnitude), and one or more ground motion attenuation models. The importance of the choices about seismogenic zonations and ground motion prediction equations has been widely focused by some sensitivity analysis (e.g., Rebez and Slejko, 2000; Barani *et al*., 2007) as the most influent parameters in a seismic hazard assessment according to the seismotectonic probabilism approach.

Uncertainty quantification (McGuire, 1977; McGuire and Shedlock, 1981; Toro *et al*., 1997) represents a crucial point in probabilistic seismic hazard analysis (PSHA) and both the aleatory variability (randomness of natural phenomena) and the epistemic uncertainty (limited quantity of data and insufficient knowledge about the earthquake process) are taken into account respectively with proper standard deviations of the used parameters and the use of a suitable logic tree (Kulkarni *et al*., 1984; Coppersmith and Youngs, 1986).

A simple logic tree with only six branches (Figure 1) has been considered in the present study: two branches account for the epistemic uncertainty in the zonation model and three branches are related to alternative ground motion prediction equations.

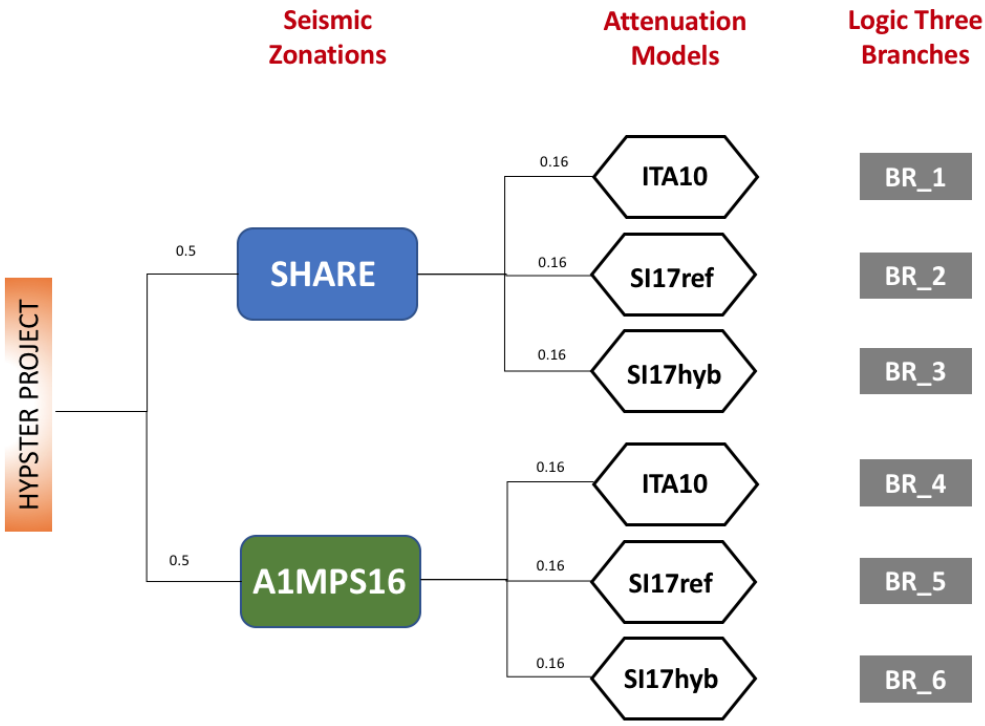

Figure 1. Logic tree used to evaluate the seismic hazard of the Southern Calabria and Sicily

Zonations geometry definition

In the present study, the used seismic sources are wide seismogenic zones (SZs), in agreement with the previous zonations [ZS4 by Meletti *et al*. (2000) and ZS9 by Meletti *et al*. (2008)] used for the Italian seismic hazard maps (Stucchi *et al*., 2011).

The first zonation of our logic tree (SHARE in Figure 1; Woessner *et al*., 2015) proposed and applied for the computation of the European seismic hazard map, has been choiced because the seismogenic information (in terms of zonation and associated seismicity rates) used as input for one of the source models considered for the SHARE map and that used for the MPS04 map are very similar (Meletti et al., 2014).

The second zonation (A1MPS16 in Figure 1; Santulin *et al.*, 2017) used in this study has been developed with the aim of applying it as a branch of the logic tree that will be used for the new Italian seismic hazard map (MPS16), presently in preparation according to the approach of the seismotectonic probabilism. With respect to the zonation ZS9 (Meletti *et al*., 2008), used for the present official seismic hazard map of Italy MPS04 (Stucchi *et al*., 2011), this zonation considers narrower sources and it is based on new and updated seismological data of the CPTI15 catalogue (Rovida *et al*., 2016). In fact, this new zonation A1MPS16 is generally more detailed (Figure 2) if compared to ZS9 (Meletti *et al*., 2008), and has deeply taken into consideration the zonation ZS4 (Meletti *et al*., 2000). The main novelties of the A1MPS16 zonation are:

• a division of some very large ZS9 zones which, in the opinion of the authors, include seismogenic structures with different geometry and failure mechanisms (see differences between the SHARE and A1MPS16 zonations in Figures 2a);

• the introduction of new SZs including areas not considered seismogenic until now.

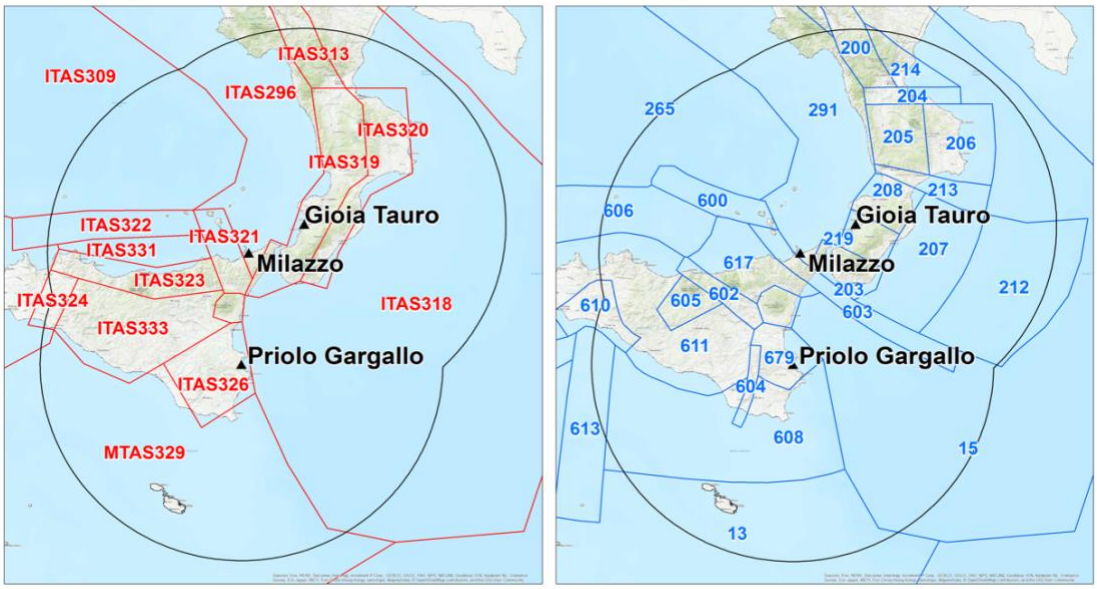

Figure 2. Seismogenic Zones used in this study that follow within a buffer of 200km around the three sites of interest: (a) SHARE, (Woessner *et al*., 2015); (b) A1MPS16, (Santulin *et al.*, 2017).

The area of Mt. Etna presents seismicity, features of surface faulting and attenuation of ground motion which are quite peculiar and for this reason it has not been discussed in this study. Here a brief description of the main zones involved in the present study, concerning the two branches of the logic tree:

- For the SHARE zonation:
  The Calabrian zones up to the Strait of Messina are two, one on the Tyrrhenian side of the region (ITAS319 zone) and one on the Ionian side (ITAS320 zone). The existence of these two distinct areas reflects very different levels of seismicity. The earthquakes with higher magnitude have in fact affected the ITAS319 zone while on the Ionian side of Calabria only 4 events have exceeded a magnitude value of 6. Extensional mechanisms are expected for these two areas, as a result of the superficial response to the flexural retreat of the Adriatic lithosphere.
  The areas identified in Sicily show a high level of simplification. The ITAS321 zone includes structures known essentially from geophysical exploration: faults linked to the "junction" that allows the backwardness of the Calabrian arc and the "synthetic" structures that segment the Gulf of Patti, similarly to what happens more to the west in the basin of Cefalù. The ITAS322 contains a fault system that extends from the westernmost part of the Aeolian Islands to the Ustica one, with an E-W orientation. This area is commonly considered to have a prevalently transcurrent character. The geometry of the ITAS323 zone is difficult to define, because the automatic epicentral determination techniques used for the catalog tend to locate on the coast all the historical earthquakes that affected it. It should also be remembered that earthquakes recorded in the last 30 years seem to indicate that the seismic activity of the ITAS322 zone is much higher than that of the northern Sicilian coast and its immediate offshore

(ITAS323 zone). It is therefore likely that some medium-strong historical earthquakes, whose intensity distributions are hardly attributable to events located on the mainland, can be referred to the already mentioned fault system of the ITAS322 zone. The ITAS324 zone is characterized by a single large seismic sequence, but the geological informations available do not provide conclusive data regarding the geometry of this source. Within the ITAS326 zone fall events of high magnitude, predominantly characterized by transcurrent mechanisms with a variable extensional component. Finally, for the ITAS323 zone, the prevailing transcurrent faulting style, that characterizes also the ITAS322, is adopted.

- For the A1MPS16 zonation:

  200 – It is characterized by strong seismicity (Mmax 7.0) developed on normal fault systems.

  203 – This zone includes the southernmost part of Calabria and northeasternmost sector of Sicily, i.e. the area hit by the so-called Messina earthquake (Mw = 7.1, 28 December 1908; Pino et al., 2009 and references therein), likely the strongest event of Italy.

  204 – This transverse zone has been individuated based on the presence of E-W trending high angle active normal faults occurring in the Crati basin. Moreover, this zone determines an interruption between the long Southern Apennine zone (200) to the north and the other zones of Calabria to the south.

  205 – This zone corresponds to the northern portion of the inner sector of Calabria, which is characterized by normal faulting along west-dipping structure.

  206 – This zone corresponds to the external sector of the previous inner zone (205). It includes the northern part of the Calabrian arc accretionary wedge, which is characterized by active N-S trending thrust fault dipping 20-40° to the west.

  207 – This zone mainly encompasses the Calabrian arc accretionary wedge that develops in the Ionian Sea. Thus, the major active fault consists of N-S to ENE-WSW striking low-angle thrust faults generally dipping towards west or NNW.

  208 – Similarly to the zone 205, this zone is affected by active normal faulting.

  212 – This zone mainly encompasses the Calabrian arc accretionary wedge that develops in the Ionian Sea. Thus, the major active fault consists of N-S to ENE-WSW striking low-angle thrust faults generally dipping towards west or NNW.

  213 – This zone includes E-W almost vertical active strike-slip faults, which likely represent transfer zones of the inner active normal faults.

  214 – This small zone can be considered as a link zone between the zone 200 characterized by active normal faulting and the transverse 204 zone. In other words, this zone links the southern Apennines to the Calabrian Arc (Ferranti et al., 2014) and is characterized by NW-SE trending, NE-dipping active thrust faults.

  219 – This zone is located in the southern part of Calabria and mainly includes NNE-SSW striking normal faults 20-40° dipping towards ESE. Moreover, at the northern and southern limit of the zone are present active transverse structure with normal to strike-slip kinematics.

  600 – This zone corresponds to a transpressional, WNW-ESE trending belt in the southeastern Tyrrhenian domain (Finetti and Del Ben, 1986). It develops in the vicinity of Alicudi, Filicudi and Salina Islands as far the area between Lipari and Vulcano

Islands where strong geodetic contraction (up to 3 mm/yr see Barreca et al., 2014) occurs. Available fault plane solutions indicate strike-slip transpressional deformation.
602 - Focal solutions highlight that seismic faulting along the analyzed belt predominantly occurs by strike-slip, normal, and subordinately by reverse oblique kinematics. The main seismogenic structures, not clearly outcropping, could be large and sub-crustal strike-slip to normal fault segments.
603 – The zone is characterized by important NW-SE trending transtensional structures extending from the Volcano Island in the Tyrrhenian sea to the Calabrian offshore crossing transversally the Peloritani mountain belt in the NE corner of Sicily This fault system probably extend in the Ionian offshore forming the Ionian fault (Polonia et al., 2016), that could correspond to the present-day lateral boundary of the Ionian lithospheric slab with earthquakes mostly occurring in the depth-range 40–70 km and characterized by extensional kinematics (Neri et al., 2009).
604 – This zone corresponds to a well-known wrenching tear structure, the Scicli–Ragusa Fault System (Ghisetti and Vezzani, 1980; Grasso and Reuther, 1988) slicing transversally the western sector of the Hyblean Plateau.
605 - This zone falls south of the Madonie Mts. in Sicily and is characterized by moderate seismicity, related to strike-slip and reverse-oblique kinematics.
606 – This zone corresponds to a narrow E-W trending contraction belt running from the NW termination of the Sicily Channel to the Aeolian Islands.
679 - Historical and instrumental records show significant seismicity along this zone. According to the strong geodetic contraction currently acting in the area (Mattia et al., 2012; Palano et al., 2012), the norther sector of the Hyblean Plateau and the Catania Plain could be characterized by blind frontal thrusting of the chain and by positive tectonic inversion of previous normal faults of the foreland margin. In this sector, seimogenic faults mostly show NE-SW trend.
608 – The Sicily Channel zone is located on the northern edge of the African continental promontory. This zone is considered as an example of continental rift (Civile et al., 2010) with diffuse normal faulting bordering graben structures.
610 –Seismically, the zone is characterized by low intensity and rare seismic activity. Quaternary potentially active faults are reverse and mainly dip to the NW.
611 - This is a compressional seismotectonic province, which extends along the Sicilian thrust and fold belt.
613 – Most of the seismicity in the Sicily Channel occurs along a broad N-S oriented belt. This belt has been interpreted as a lithospheric transfer fault zone between two segments of the rift system.
617 – Although this zone doesn't show remarkable evidence of active tectonic on the surface, it is characterized by frequent and low magnitude seismic events. and it is characterized by prevalent focal solutions with normal kinematic trending as a whole NE-SW.

Zonations seismicity definition

Once defined the zonation geometries involved in the computation, it is necessary to compute also their seismic characterization. For the scope of the SHARE project a new homogeneous earthquake catalogue was compiled (SHEEC—the "SHARE European Earthquake Catalogue"; Stucchi et al., 2012; Grünthal et al., 2013). For the A1MPS16 zonation the new version of the Italian Parametric Catalogue CPTI15 (Rovida et al., 2016) has been the only seismological source.

Concerning the node relative to the seismicity model, to compute the values of the GR coefficients (a and b-values), different methodologies for assessing the b-value are available in literature. In this work the Maximum Likelihood (ML) method (GR-ML) has been adopted, according to the formulation proposed by Weichert (1980): a general routine that accounts also for different completeness periods for the various magnitude classes of the earthquakes in the catalogue. For the SHARE branch, the rates of the zones are the original ones. For the A1MPS16 branch, since some small areas were poor in events, the corresponding GR b-values were in some cases abnormal values, far from the theoretical "world" value of 1. For this reason, it was chosen to merge zones in homogeneous areas, using the information available, mainly the type of failure mechanism, and the completeness and Mmax macroareas. For these homogeneous areas, the b-value was calculated, while the zones were kept independent for the a-value computation.

The Mmax values have been identified on the basis of the maximum observed or estimated earthquake in each SZ and increasing those estimates by the related standard deviation.

Table 1. Seismic characterization of each SHARE zone. **FM**: Focal Mechanism; **NF**: Normal Faulting; **RF**: Reverse Faulting. **h**: reference depth. **ASC**: Active Shallow Crust; **SSC**: Stable Shallow Crust.

Id	a	b	Mmin	Mmax	FM	h [km]	Tectonics
ITAS296	4.00	1.00	4.7	6.6	RF	13.2	ASC
ITAS318	3.90	1.00	4.7	8	RF	13.2	ASC
ITAS319	3.90	0.90	4.7	7.7	NF	11.4	ASC
ITAS320	4.00	1.00	4.7	7.7	NF	11.4	ASC
ITAS321	4.30	1.10	4.7	7.7	NF	13.2	ASC
ITAS322	3.90	1.00	4.7	7.7	RF	13.2	ASC
ITAS323	4.30	1.10	4.7	6.6	RF	9.1	ASC
ITAS324	3.90	1.09	4.7	6.6	RF	9.1	ASC
ITAS326	2.80	0.80	4.7	7.7	RF	13.2	ASC
MTAS329	3.90	1.00	4.7	6.6	RF	13.2	ASC
ITAS331	0.18	0.99	4.7	6.6	RF	13.2	ASC
ITAS333	4.20	1.10	4.7	6.6	RF	13.2	ASC
ITAS309	3.60	1.00	4.7	6.5	RF	10	SSC

Table 2. Seismic characterization of each A1MPS16 zone. **FM**: Focal Mechanism; **NF**: Normal Faulting; **RF**: Reverse Faulting. **h**: reference depth. **ASC**: Active Shallow Crust; **SSC**: Stable Shallow Crust.

Id	a	b	Mmin	Mmax	FM	h [km]	Tectonics
617	4.50	1.25	4.5	6.4	NF	17	ASC
602	4.57	1.25	4.5	5.8	SS	15	ASC
604	2.30	0.85	4.5	5.5	SS	25	ASC
606	3.34	0.96	4.5	6.4	RF	10	ASC
610	2.81	0.96	4.5	6.7	RF	15	ASC
611	3.32	0.96	4.5	5.8	RF	5	ASC
613	2.98	0.85	4.5	5.2	SS	10	ASC
605	2.85	0.96	4.5	5.8	RF	15	ASC
603	4.42	1.25	4.5	6.4	SS	10	ASC
600	4.85	1.25	4.5	5.5	SS	17	ASC
608	2.30	0.85	4.5	5.2	SS	10	ASC
679	2.28	0.85	4.5	7.6	RF	12	ASC
219	1.71	0.70	4.5	7.3	NF	7	ASC
200	2.67	0.73	4.5	7.6	NF	10	ASC
204	3.14	0.97	4.5	6.4	NF	9	ASC
205	2.17	0.70	4.5	7.3	NF	9	ASC
206	2.89	0.97	4.5	7	RF	8	ASC
208	1.98	0.70	4.5	7	NF	8	ASC
203	1.89	0.70	4.5	7.3	NF	8	ASC
214	2.39	0.97	4.5	5.8	RF	10	ASC
213	2.67	0.97	4.5	6.4	SS	12	ASC
212	2.52	0.85	4.5	5.5	RF	10	ASC
207	2.52	0.85	4.5	5.5	RF	30	ASC
265	3.60	1.00	4.5	6.5	RF	10	SSC
291	3.99	1.00	4.5	6.6	RF	13.2	ASC
13	3.52	0.87	4.5	5.8	RF	10.2	ASC
15	3.89	1.00	4.5	8	RF	10.2	ASC

GMPEs

Concerning the node relative to the GMPEs, one branch is related to the ITA10 (*Bindi et al.,* 2011), calibrated with Italian accelerometric data, while the other two branches are for the empirical (SI17ref) and the hybrid (SI17hyb) region specific attenuation models, calibrated for the study area [see the Deliverables of Task 2 (D'Amico et al., 2018), and Task 3 (Lanzano et al., 2018)]. All the branches are equally weighted to highlight the influence of the different SZs and GMPEs on the hazard assessment.

Figure 3a and Figure 3b show an example of magnitude scaling of the PGAs considering the three GMPEs used for PSHA, defined, respectively, for a normal and reverse mechanism.

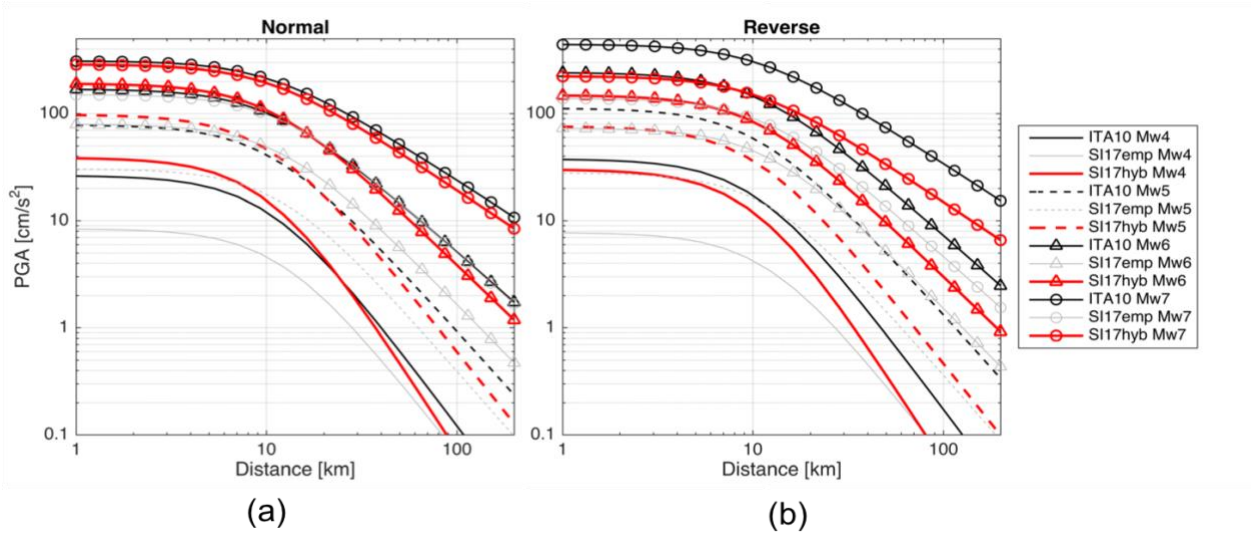

Figure 3. GMPEs used in the logic tree plotted for different moment magnitudes (from 4 to 7) and for normal (**a**) and reverse (**b**) fault; black lines for the ITA10 (Bindi et al., 2011), gray lines for SI17ref and red lines for SI17hyb.

Results

The computer program CRISIS 2015 (Ordaz et al., 2013) has been employed for the computation of the expected ground motion in terms of maps, curves and uniform hazard response spectra (UHRS). Figure 4 represents the hazard maps at various T_R (from 100 to 3900yrs) for PGA, and SA at 0.3 and 1 s, respectively. As expected the hazard level enhances with the increase of return period T_R, presenting similar behavior at all periods. In particular, the Hyblean Mountains area (ITAS326 in SHARE and SZ679 in A1MPS16, see Figure 2) steps from very low levels of hazard at lower T_R, to values comparable to the maximum values obtained in Calabria, at higher T_R. This behavior can be related to the low b-value of the GR (see Table 1 and Table 2), due to the occurrence of several historical earthquakes of high magnitude.

The seismic parametrization also influences the difference in PSHA between Milazzo (i.e. SZ291 in A1MPS16 b=1) and Priolo Gargallo (i.e. SZ679 in A1MPS16 b=0.85). Figure 4 shows an increasing seismic hazard for the latter site, highlighted by the crossing of the hazard curves of Milazzo and Priolo Gargallo (Figure 5). It should be noted a progressive increase in the

return period at which the crossing of the two hazard curves occurs, moving from the PGA to higher spectral ordinates. The same inversion in the hazard behavior between Milazzo and Priolo Gargallo can be observed by comparing the UHRSs in Figure 6. In general, the highest levels of seismic hazard are in case of Gioia Tauro (Figure 5 and Figure 6), with a maximum of about 1g for T_R=3,900yrs and SA=0.3s.

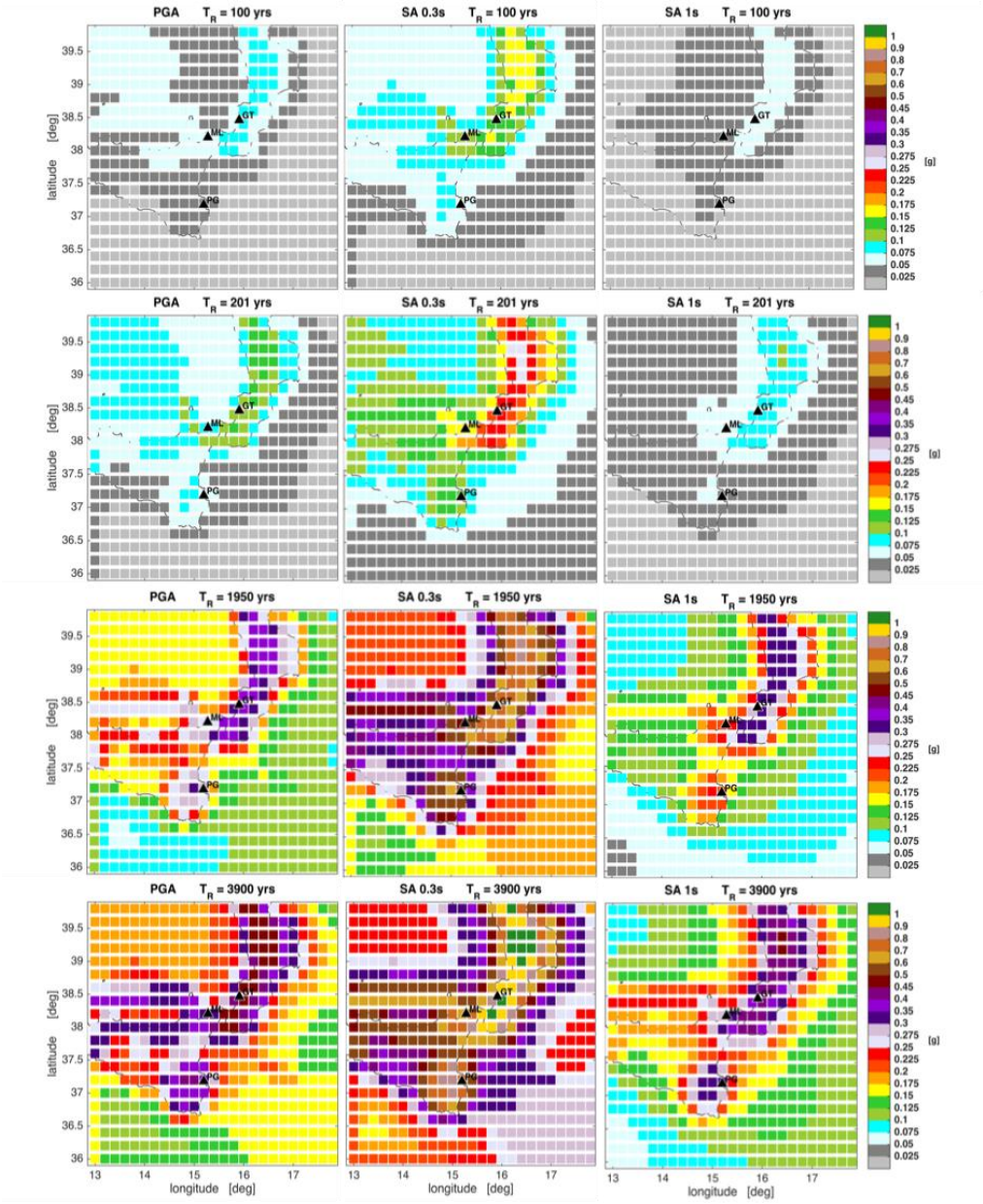

Figure 4. Hazard map computed for different intensity measures (PGA and SA at 0.3 and 1 s) and for various return periods (T_R) merging all the branches of the logic tree (see Figure 1).

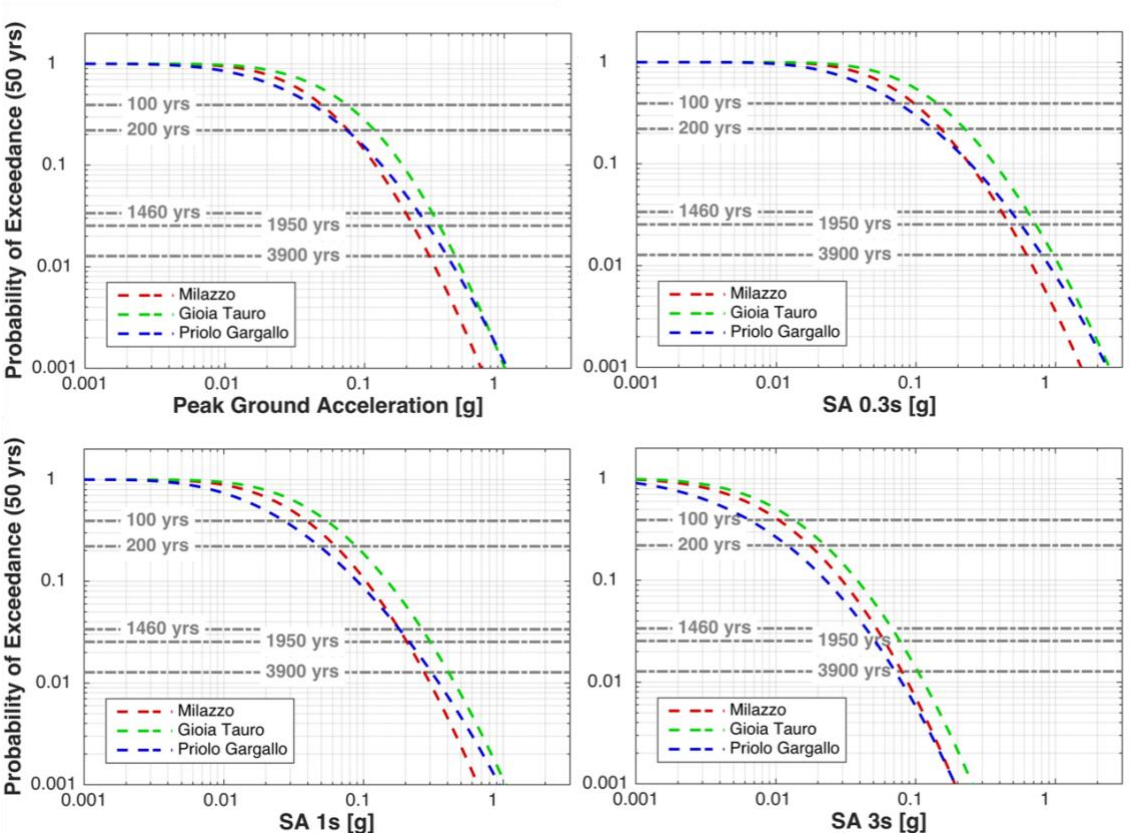

Figure 5. Probability of exceedance (50yrs) for the three sites of interest calculated for PGA, SA at 0.3, 1, and 3 s, considering all the logic tree branches (see Figure 1).

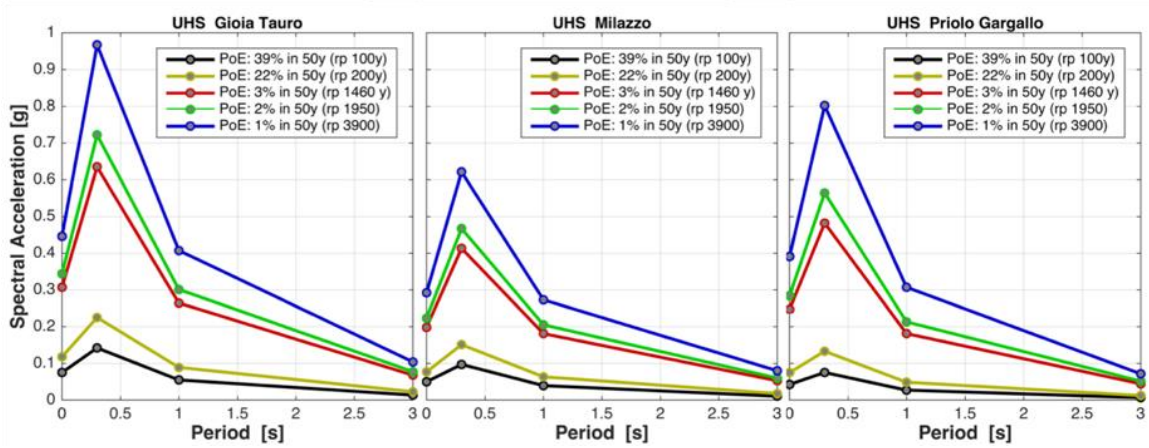

Figure 6. Uniform Hazard Spectra (UHS) for the three sites of interest obtained for different probabilities of exceedance. UHS amplitudes are for PGA, and SA at 0.3, 1, and 3 s.

The results of this study for PGA are compared with those of the current Italian national hazard map MPS04 (Figure 7). Although they are not directly comparable in terms of numerical results, because different input elements have been used (for example different catalogues and GMPEs), the general behavior of the hazard curves for the three sites is similar in both studies (Figure 7), thus supporting the validity of our approach.

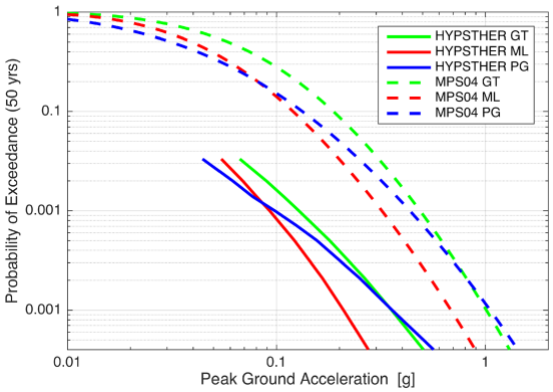

Figure 7. Hazard curves in terms of PGAs for the tree sites of interest derived from the Italian hazard official map (MPS04, http://esse1-gis.mi.ingv.it/) and computed in this study (HYPSTHER) by using the logic tree in Figure 1.

As the final aim of this study is to explore the possibility of using hybrid GMPEs in region-specific PSHA, we analyze the influence of different typologies of attenuation models (among empirical or hybrid ones) by comparing the PGA hazard curves of the three branches of Figure 1 correspondent to the A1MPS16 node (Figure 8). The behavior of the other spectral periods is also shown in Appendix D (Figure D2).

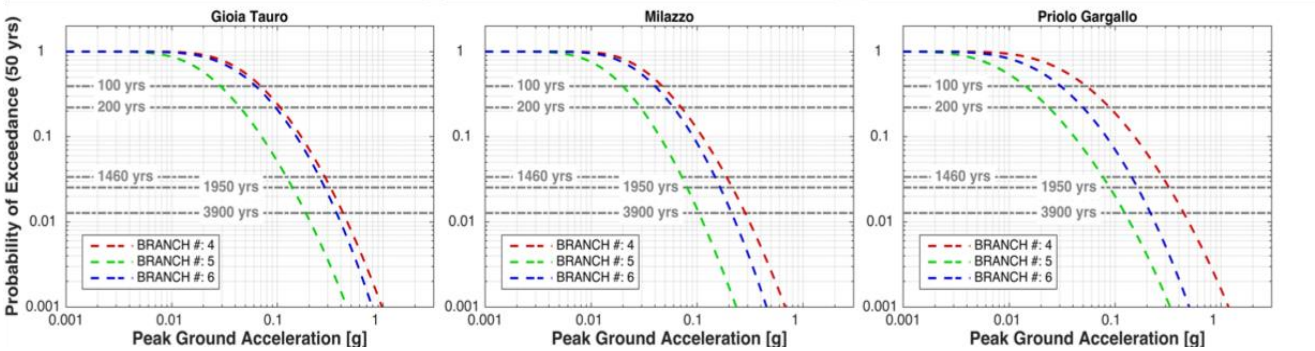

Figure 8. Probability of exceedance (50yrs) for the three sites of interest calculated for PGA considering the logic tree branches related to the A1MPS16 node (see Figure 1).

Focusing our attention on differences between ITA10 (BRANCH#: 4) and region-specific hybrid model (SI17hyb, BRANCH#: 6), we observe a reduction of the hazard levels up to 10% for Gioia Tauro, up to 20% for Milazzo, and up to 50% for Priolo Gargallo at T_R = 3900 yrs. Hazard levels for SI17ref (BRANCH#: 5) are instead remarkably lower. For Gioia Tauro, the differences between BRANCH#: 4 and BRANCH#: 6 are small both for SLD (T_R = 100yrs) and SLC (T_R = 1950). This is because the main contribution to the hazard derives from normal earthquakes 10 km far from the site and characterized by moment magnitudes around 5.0 and 6.0, respectively (see the de-aggregation results in Appendix F). In both cases, the median values of ITA10 and SI17hyb are almost identical (Figure 3a) but the standard deviation associated to the hybrid model is slightly lower (see Task 3, Lanzano et al., 2018). Differently from Gioia Tauro, the SZs of Milazzo and Priolo Gargallo are characterized by reverse faulting

(Table 2). As a result, because the ITA10 model is systematically higher than SI17hyb (Figure 3b), the BRANCH#: 4 hazard levels for SLD (T_R = 200 yrs) and SLC (T_R = 3900 yrs) are always higher than those related to the BRANCH#: 6.

Conclusions

The empirical (SI17ref) and hybrid (SI17hyb) prediction models, derived from Task 3 (Lanzano et al., 2018), and the reference GMPEs for Italy (ITA10, Bindi et al., 2011) have been used for hazard calculation in a simple logic tree with only six branches (two branches for the epistemic uncertainty in the zonation model). Testing the performance of region-specific GMPEs for magnitude-distance pairs poorly sampled by recorded data, we highlighted a variability of the seismic hazard in terms of probability of exceedance of the ground motion parameter (i.e. PGA) due to the use of different attenuation models.

The impact on the seismic design of some critical infrastructures, such as ports (Gioia Tauro), refineries (Milazzo) or chemical plants (Priolo Gargallo) located along the shoreline of the investigated area, has been assessed. Using the region-specific hybrid model, a reduction of the hazard levels is observed, up to 50% for Priolo Gargallo for SLC, with respect to ITA10. Hazard levels for SI17ref are instead lower than SI17hyb, due to the change of the median predictions in near-fault conditions. The highest levels of seismic hazard are observed for the site of Gioia Tauro, with a 1g at SA=0.3s for SLC.

This approach is timely for updating the next generation seismic-hazard maps (i.e. the new release of the Italian seismic hazard map MPS16, http://tinyurl.com/jg99xsc), including hybrid GMPEs in areas where recordings are few and ground motion models are not well constrained, especially in near field conditions. The region-specific hybrid GMPEs can have a strong impact on seismic design and retrofitting of critical infrastructure both for damage and collapse limit states.

References

Barani S., Spallarossa D., Bazzurro P., Eva C.; 2007: Sensitivity analysis of seismic hazard for Western Liguria (North Western Italy): A first attempt towards the understanding and quantification of hazard uncertainty. Tectonophysics, Volume 435, 1–4, 13-35. ISSN 0040-1951, http://dx.doi.org/10.1016/j.tecto.2007.02.008.

Barreca G., Bruno V., Cultrera F., Mattia M., Monaco C., Scarfì L.; 2014; New insights in the geodynamics of the Lipari–Vulcano area (Aeolian archipelago, southern Italy) from geological, geodetic and seismological data. J. of Geodynamics, 82, 150-167, Doi: 10.1016/j.jog.2014.07.003.

Bindi, D., Pacor, F., Luzi, L., Puglia, R., Massa, M., Ameri, G., Paolucci R. (2011) Ground motion prediction equations derived from the Italian strong motion database. Bulletin of Earthquake Engineering. Volume: 9, Issue: 6, Special Issue: SI, Pages: 1899-1920, DOI: 10.1007/s10518-011-9313-z.

CEN (2004): Design of structures for earthquake resistance, Part 1: General rules, seismic actions and rules for buildings, EN 1998-1, European Committee for Standardization (CEN), Brussels, http://www.cen.eu/cenorm/homepage.htm.

Civile D., Lodolo E., Accettella D., Geletti R., Ben-Avraham Z., Deponte M., Facchin L., Ramella R., Romeo R.; 2010: The Pantelleria graben (Sicily Channel, central Mediterranean): an example of intraplate 'passive' rift. Tectonophysics, 490,173–183.

Cornell C. A.; 1968: Engineering seismic risk analysis. Bull. Seism Soc. Am., 58, 1583-1606.

CS.LL.PP (2008) DM 14 Gennaio 2008. *Norme Tecniche per le Costruzioni*. Gazzetta Ufficiale della Repubblica Italiana, 29 (in Italian).

D'Amico, M.; Tiberti, M.M.; Russo, E.; Gomez-Capera, A. 2018 Ground motion simulation. Istituto Nazionale di Geofisica e Vulcanologia, HYPSTHER project, http://hypsther.mi.ingv.it/ - doi: 10.5281/zenodo.1162203

Ferranti, L., P. Burrato, F. Pepe, E. Santoro, M. E. Mazzella, D. Morelli, S. Passaro, and Vannucci G.; (2014): An active oblique contractional belt at the transition between the Southern Apennines and Calabrian Arc: The Amendolara Ridge, Ionian Sea, Italy. Tectonics, 33, doi:10.1002/ 2014TC003624.

Finetti I.R., Del Ben A.; 1986: Geophysical study of the Tyrrhenian opening. Boll. Geof. Teor. Appl. 28, 75-156.

Ghisetti F., Vezzani L.; 1980: The structural features of the Hyblean Plateau and the Mount Judica area (South-Eastern Sicily): a microtectonic contribution to the deformational history of the Calabrian arc. Boll. Soc. Geol. It., 99, 55–102.

Grasso M., Reuther C.D.; 1988: The western margin of the Hyblean Plateau a neotectonic transform system of the SE Sicilian foreland. Annale Tectonicae, 2, 107-120.

Grünthal, G., Wahlström, R., Stromeyer, D. (2013): The SHARE European Earthquake Catalogue (SHEEC) for the time period 1900–2006 and its comparison to the European-Mediterranean Earthquake Catalogue (EMEC). - Journal of Seismology, 17, 4, 1339-1344. DOI: 10.1007/s10950-013-9379-y

Kulkarni R.B., Youngs R. R. and Coppersmith K. J.; 1984: Assessment of confidence intervals for results of seismic hazard analysis. In: Proceedings of the Eighth World Conference on Earthquake Engineering, July 21-28, 1984, San Francisco CA U.S.A., Prentice-Hall Inc., Englewood Cliffs NJ U.S.A., vol. 1, pp. 263-270.

Lanzano, G.; D'Amico, M.; Felicetta, C.; Puglia, R. 2018 GMPEs calibration. Istituto Nazionale di Geofisica e Vulcanologia, HYPSTHER project, http://hypsther.mi.ingv.it/ - doi: 10.5281/zenodo.1162735

Mattia M., Bruno V., Cannavò F., Palano M.; 2012: Evidences of a contractional pattern along the northern rim of the Hyblean Plateau (Sicily, Italy) from GPS data. Geol. Acta 10, 1–9. http://dx.doi.org/10.1344/105000001705.

McGuire R. K.; 1977: Seismic design spectra and mapping procedures using hazard analysis based directly on oscillator response. Earthq. Engin. Struct. Dyn., 5, 211-234.

McGuire R. K. and Shedlock K.M.; 1981: Statistical uncertainties in seismic hazard evaluations in the United States. Bull. Seism. Soc. Am., 71, 1287-1308.
Meletti, C.; Patacca, E.; Scandone P. Construction of a seismotectonic model: the case of Italy. *Pure Appl. Geophys.* 2000, *157*, 11-35.
Meletti C., Galadini F., Valensise G., Stucchi M., Basili R., Barba S., Vannucci G. and Boschi E.; 2008: A seismic source zone model for the seismic hazard assessment of the Italian territory. Tectonophysics, 450, 85–108.
Meletti, C.; Rovida, A.; D'Amico, V.; Stucchi, M. Modelli di pericolositá sismica per l'area italiana: "MPS04- S1" e "SHARE". *Progettazione Sismica* 2014, *5(1)*, 15-25, doi: 10.7414/PS.5.1.15-25.
Neri G., Orecchio B., Totaro C., Falcone G., Presti D.; 2009: Subduction beneath southern Italy close the ending: results from seismic tomography. Seim. Res. Lett., 80, 63-70.
Ordaz, M.; Martinelli, F.; D'Amico, V.; Meletti, C. CRISIS2008: A Flexible Tool to Perform Probabilistic Seismic Hazard Assessment. *Seismol. Res. Lett.* 2013, 84, 495–504, doi: 10.1785/0220120067.
Palano M., Ferranti L., Mattia M., Monaco C., Aloisi M., Bruno V., Cannavò F., Siligato G.; 2012: GPS velocity and strain fields in Sicily and southern Calabria, Italy: updated geodetic constraints on tectonic block interaction in the central Mediterranean. Journ. of Geophys. Research, 117, B07401, doi:10.1029/2012JB009254.
Pino A. N., Giardini D. and Boschi, E. (2000). The December 28, 1908, Messina Straits, southern Italy, earthquake: Waveform modeling of regional seismograms. Journal of Geophysical Research. 105. 25473-25492. 10.1029/2000JB900259.
Polonia A., Torelli L., Artoni A., Carlini M., Faccenna C., Ferranti L., Gasperini L., Govers R., Klaeschen D., Monaco C., Neri G., Nijholt N., Orecchio B., Wortel R. M. 2016: The Ionian and Alfeo-Etna fault zones: New segments of an evolving plate boundary in the central Mediterranean Sea. Tectonophysics, Doi: 10.1016/j.tecto.2016.03.016.
Rebez A. and Slejko D.; 2000: Sensitivity analysis on the input parameters in probabilistic seismic hazard assessment. Soil Dynamics and Earthquake Engineering, 20(5-8):341-351
Rovida A., Locati M., Camassi R., Lolli B., Gasperini P.; 2016: CPTI15, the 2015 version of the Parametric Catalogue of Italian Earthquakes. Istituto Nazionale di Geofisica e Vulcanologia. doi:http://doi.org/10.6092/INGV.IT-CPTI15.
Santulin, M.; Tamaro, A.; Rebez, A.; Slejko, D.; Sani, F.; Martelli, L.; Bonini, M.; Corti, G.; Poli, M.E.; Zanferrari, A.; Marchesini, A.; Busetti, M.; Dal Cin, M.; Spallarossa, D.; Barani, S.; Scafidi, D.; Barreca, G.; Monaco, C. Seismogenic zonation as a branch of the logic tree for the new Italian seismic hazard map - MPS16: a preliminary outline. *Bollettino di Geofisica Teorica e Applicata* 2017, *58*, 313-342, doi:10.4430/bgta0216.
Santulin, M., D'Amico, M.; Lanzano, G. 2018 Hazard Assessment. Istituto Nazionale di Geofisica e Vulcanologia, HYPSTHER project, http://hypsther.mi.ingv.it/
Stucchi M., Meletti C., Montaldo V., Crowley H., Calvi G.M. and Boschi E.; 2011: Seismic hazard assessment (2003–2009) for the Italian building code. Bull. Seism. Soc. Am., 101, 1885–1911. doi: 10.1785/0120100130.
Stucchi et al., 2012. The SHARE European Earthquake Catalogue (SHEEC) 1000–1899. Journal of Seismology, doi: 10.1007/s10950-012-9335-2.
Toro G. R., Abrahamson N. A. and Schneider J. F.; 1997: Model of strong motions from earthquakes in central and eastern North America: best estimates and uncertainties. Seism. Res. Lett., 68, 41-57.
Weichert D. H.; 1980: Estimation of the earthquake recurrence parameters for unequal observation periods for different magnitudes. Bull. Seismol. Soc. Am., 70, 1337-1346.
Woessner, J., L. Danciu, D. Giardini, H. Crowley, F. Cotton, G. Grünthal, G. Valensise, R. Arvidsson, R. Basili, M. N. Demircioglu, S. Hiemer, C. Meletti, R. W. Musson, A. N. Rovida, K. Sesetyan, M. Stucchi, and the SHARE consortium (2015), The 2013 European Seismic Hazard Model: key components and results. Bull. Earthq. Eng., 3:3553–3596. doi:10.1007/s10518-015-9795-1.

Appendix A

Exceedance probability curves (50 yrs) correspondent to each branch of the HYPSTHER project are reported in the following (Figures A1-A6). The hazard curves for the two branches related to the two seismogenic zonations (Figure A7 for SHARE and Figure A8 for A1MPS16, respectively) are also reported. The hazard is calculated for the three test sites (Milazzo, Gioia Tauro and Priolo Gargallo) and for four intensity measures (PGA, SA at 0.3, 1, and 3 s).

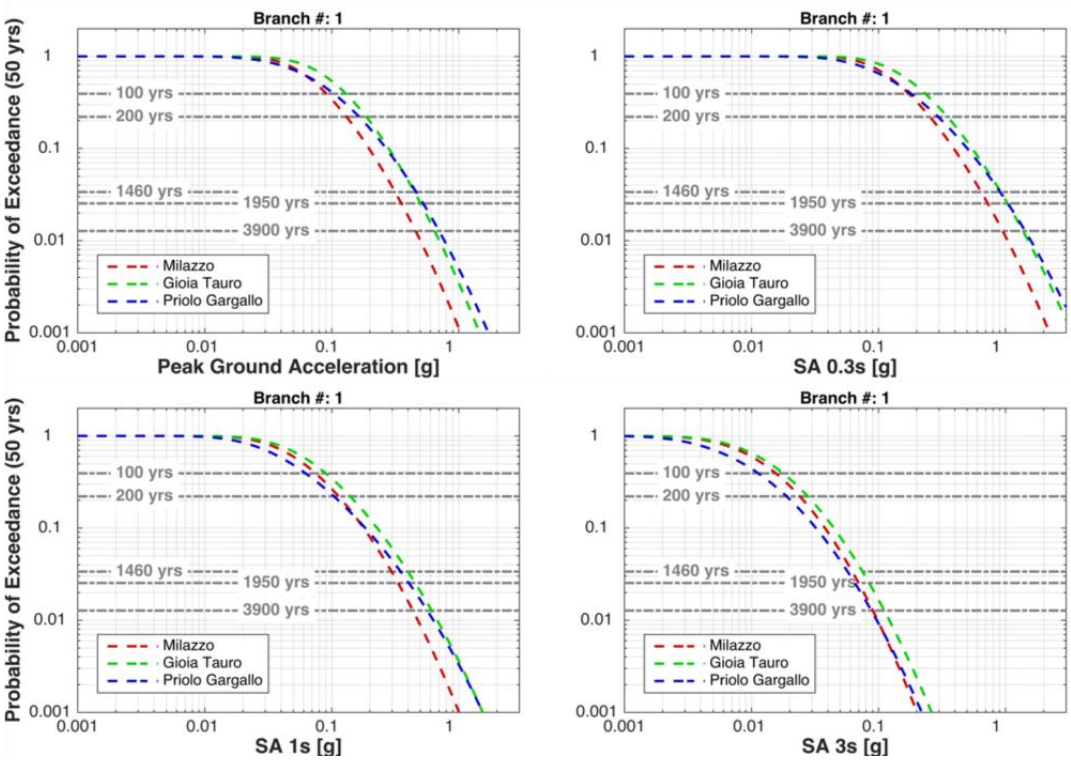

Figure A1

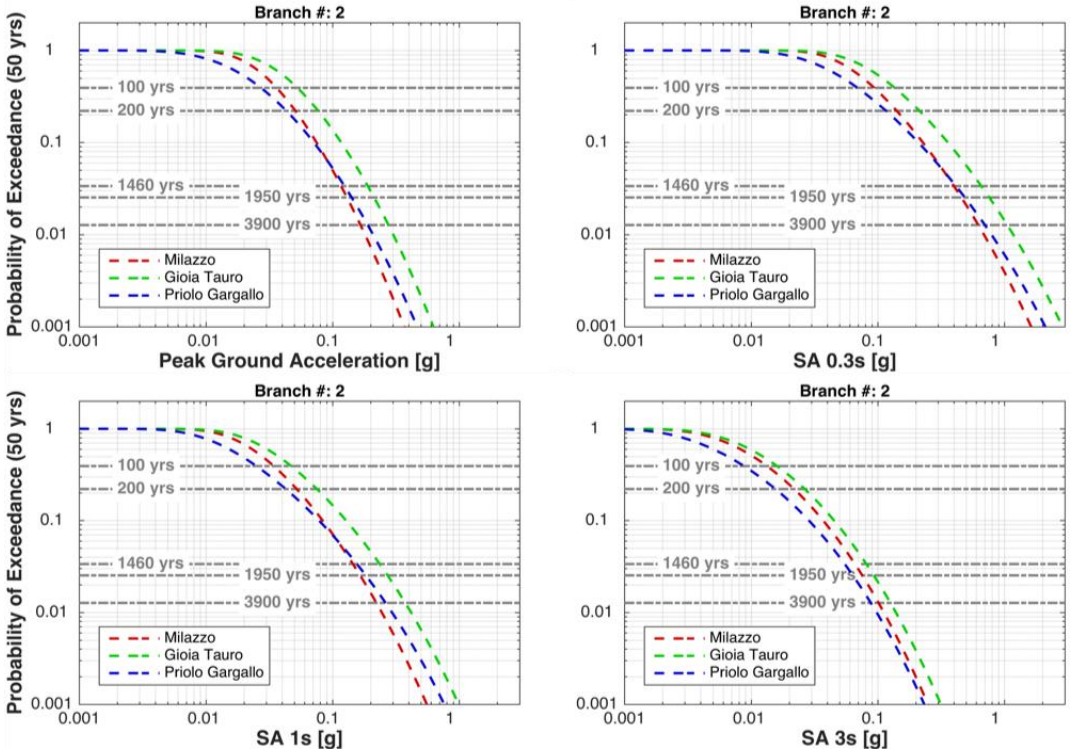

Figure A2

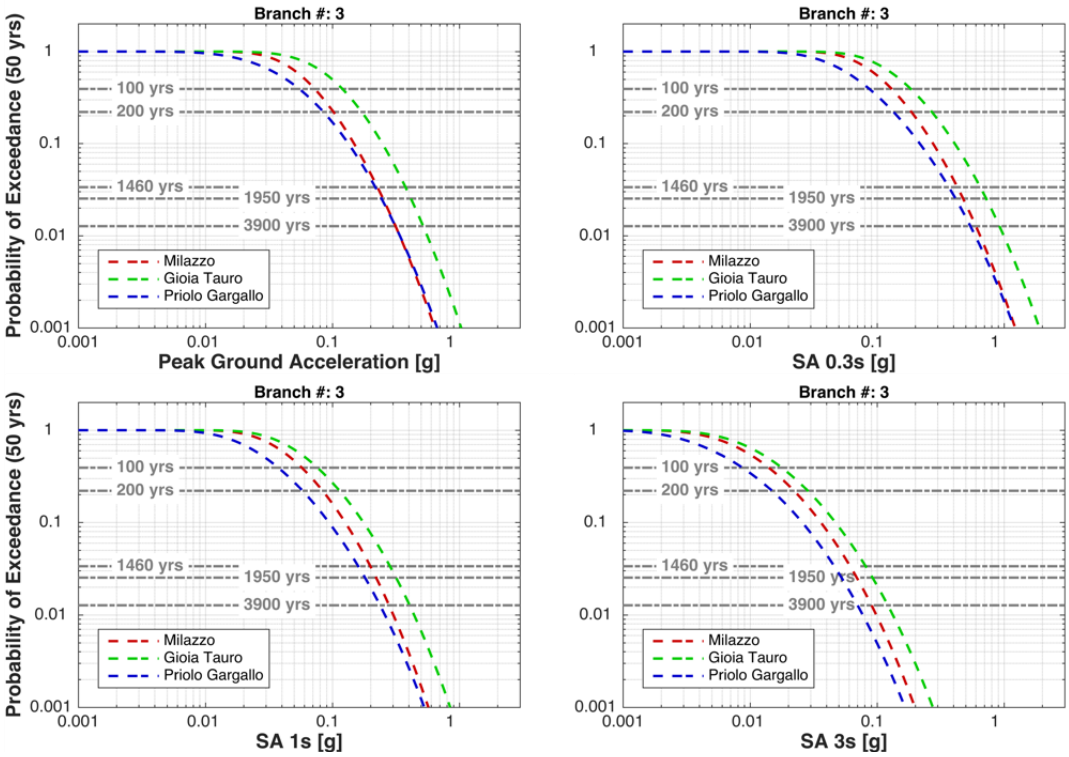

Figure A3

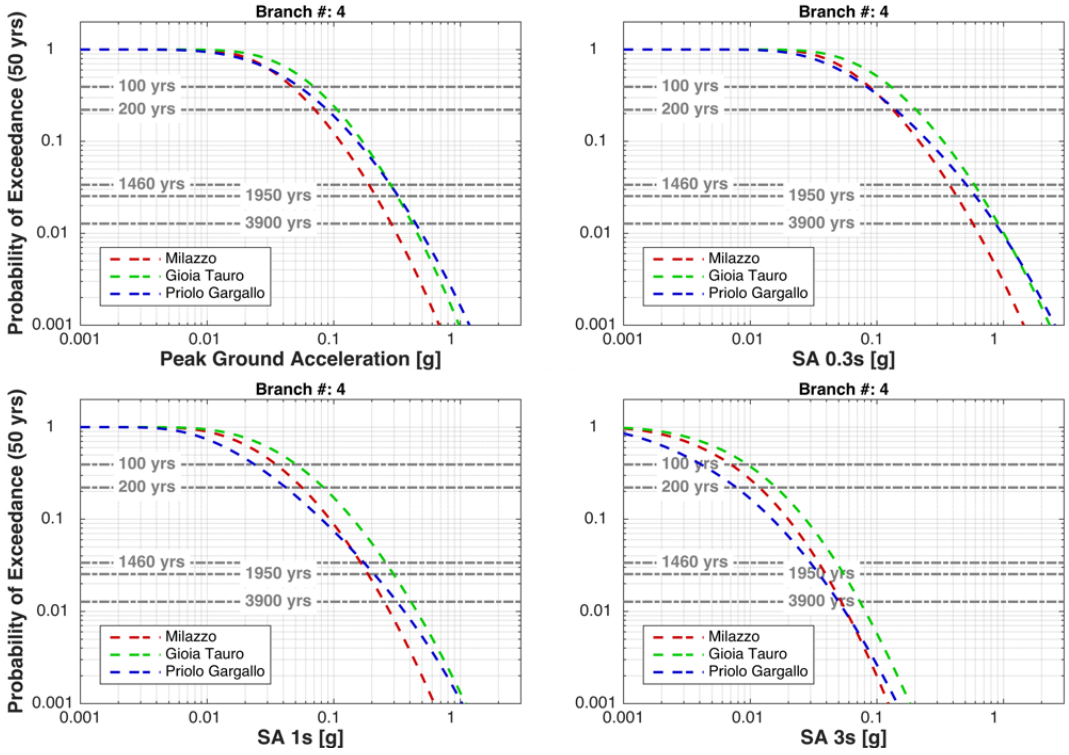

Figure A4

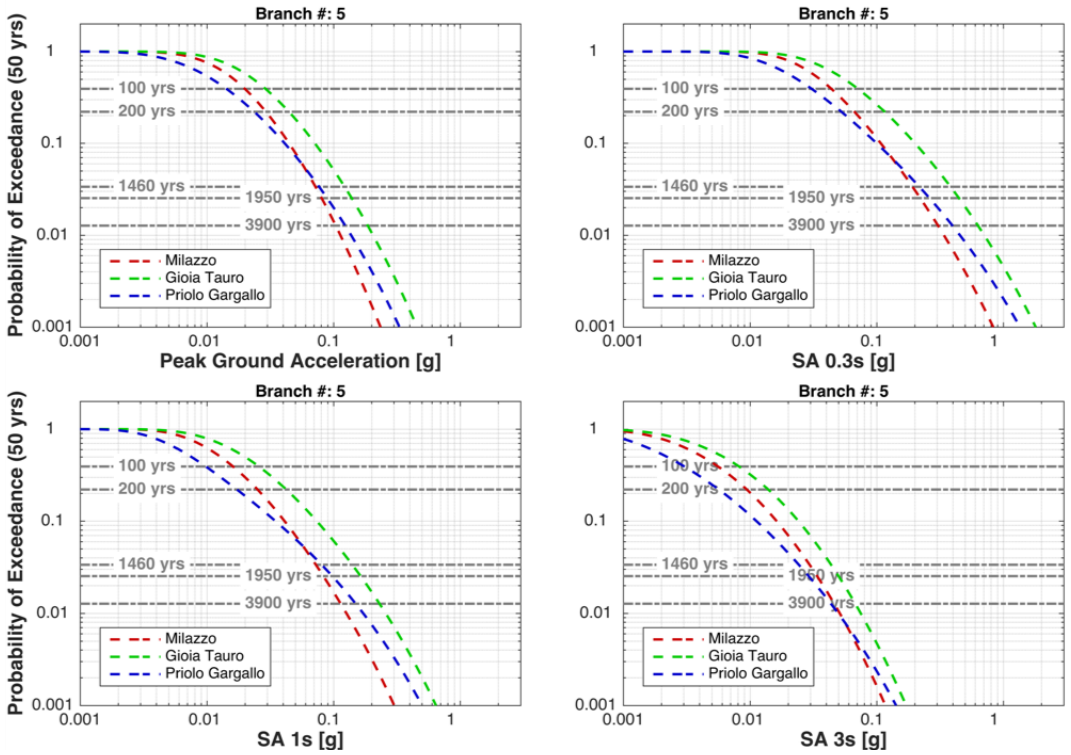

Figure A5

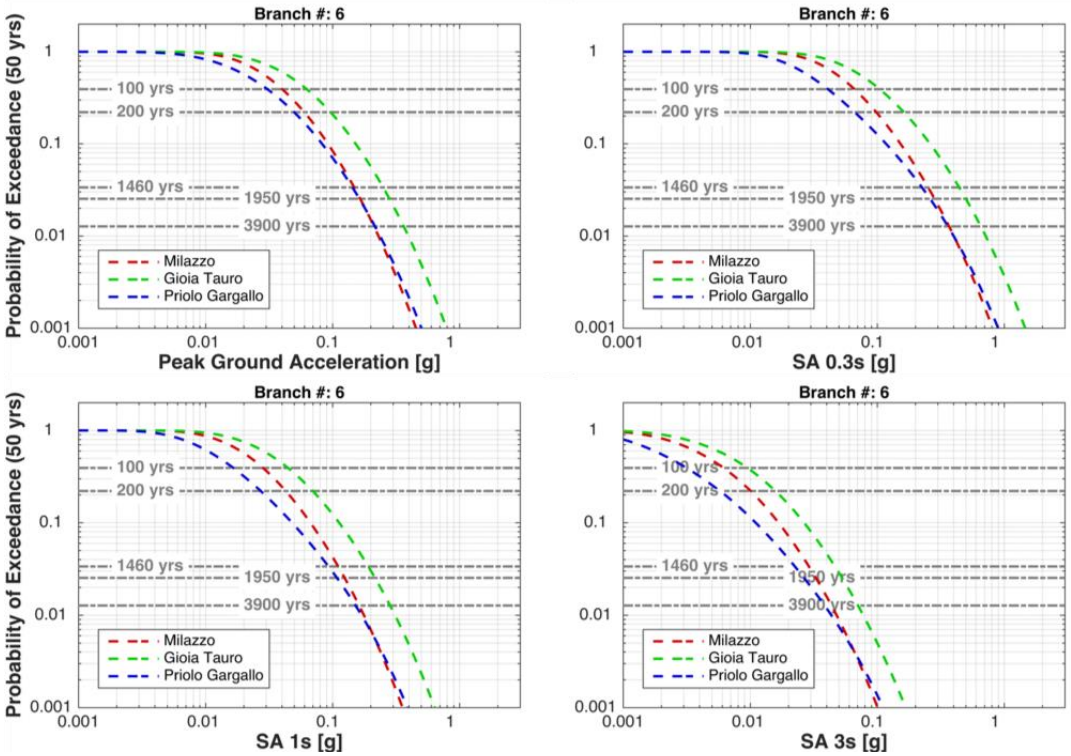

Figure A6

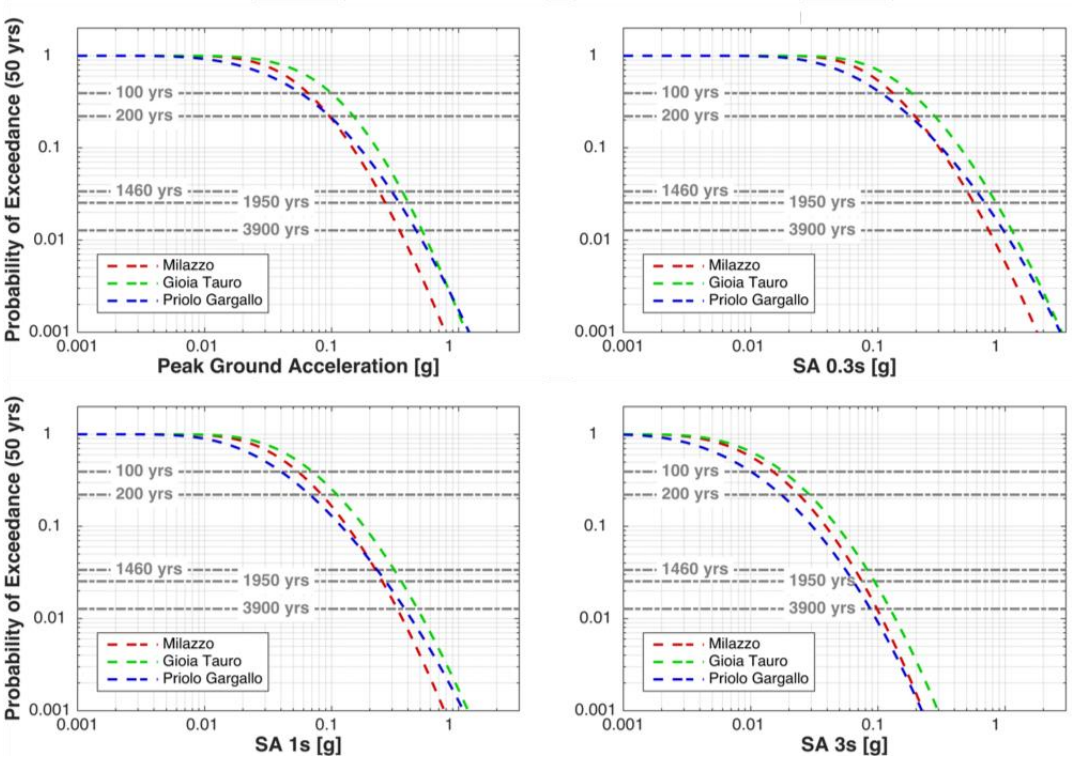

Figure A7

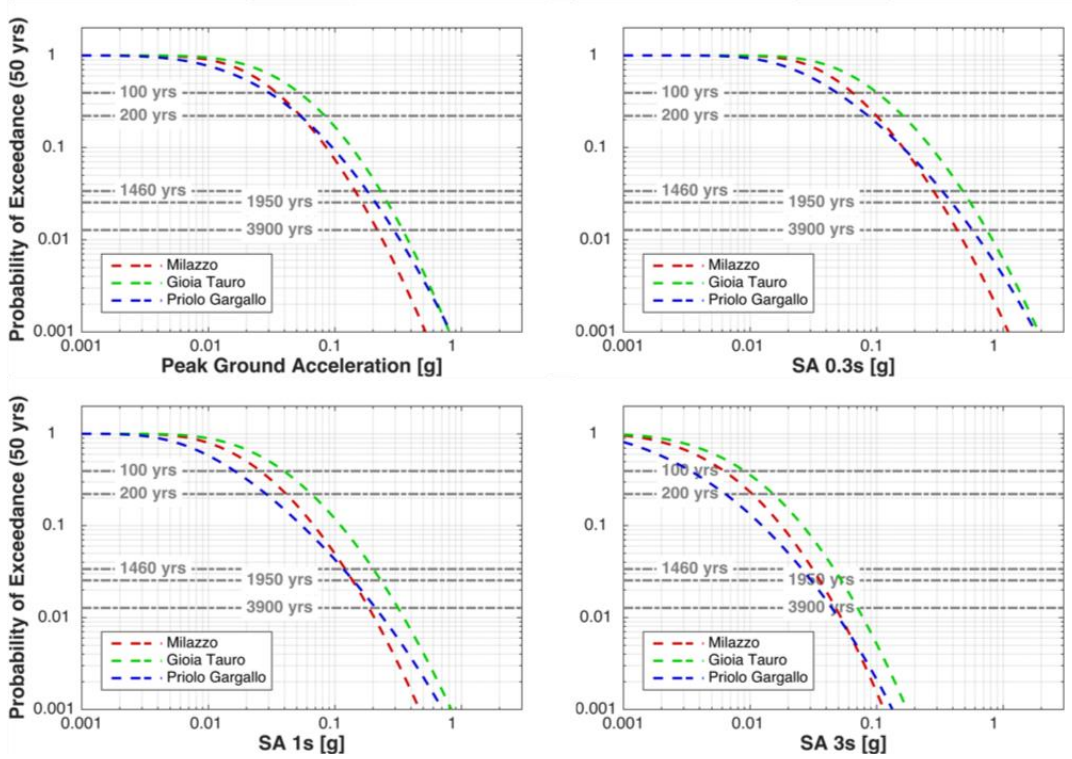

Figure A8

Appendix B

Uniform Hazard Spectra (UHS) in 50 yrs correspondent to each branch of the HYPSTHER project are reported in the following (Figure B1-B2).The UHSs for the two branches related to the two seismogenic zonations (Figure B4 for SHARE and Figure B5 for A1MPS16, respectively) are also reported. The hazard is calculated for the three test sites (Milazzo, Gioia Tauro and Priolo Gargallo) and for four intensity measures (PGA, SA at 0.3, 1, and 3 s).

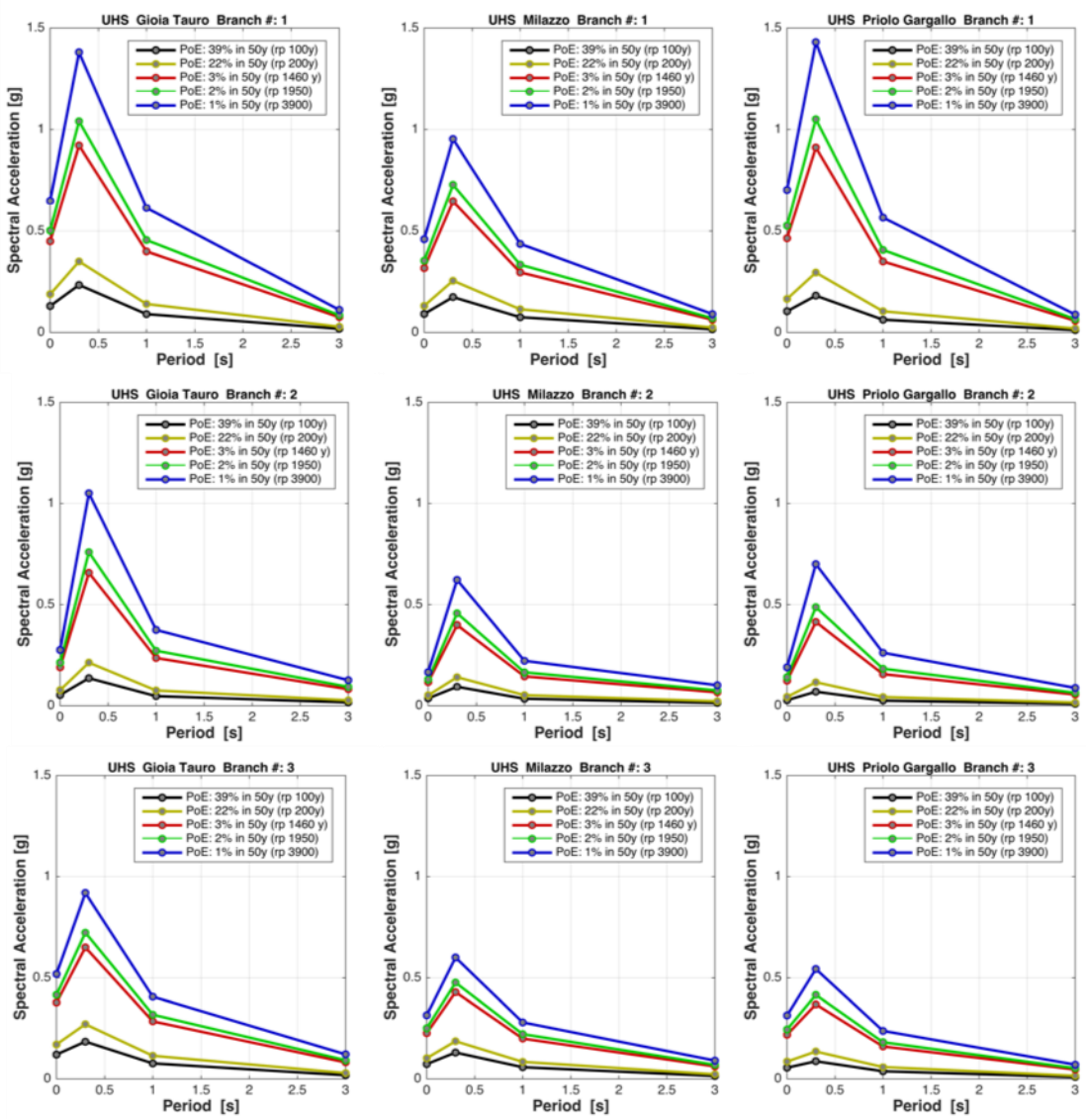
UHS Gioia Tauro Branch #: 1
UHS Milazzo Branch #: 1
UHS Priolo Gargallo Branch #: 1
UHS Gioia Tauro Branch #: 2
UHS Milazzo Branch #: 2
UHS Priolo Gargallo Branch #: 2
UHS Gioia Tauro Branch #: 3
UHS Milazzo Branch #: 3
UHS Priolo Gargallo Branch #: 3
PoE: 39% in 50y (rp 100y)
PoE: 22% in 50y (rp 200y)
PoE: 3% in 50y (rp 1460 y)
PoE: 2% in 50y (rp 1950)
PoE: 1% in 50y (rp 3900)
Spectral Acceleration [g]
Period [s]

Figure B1

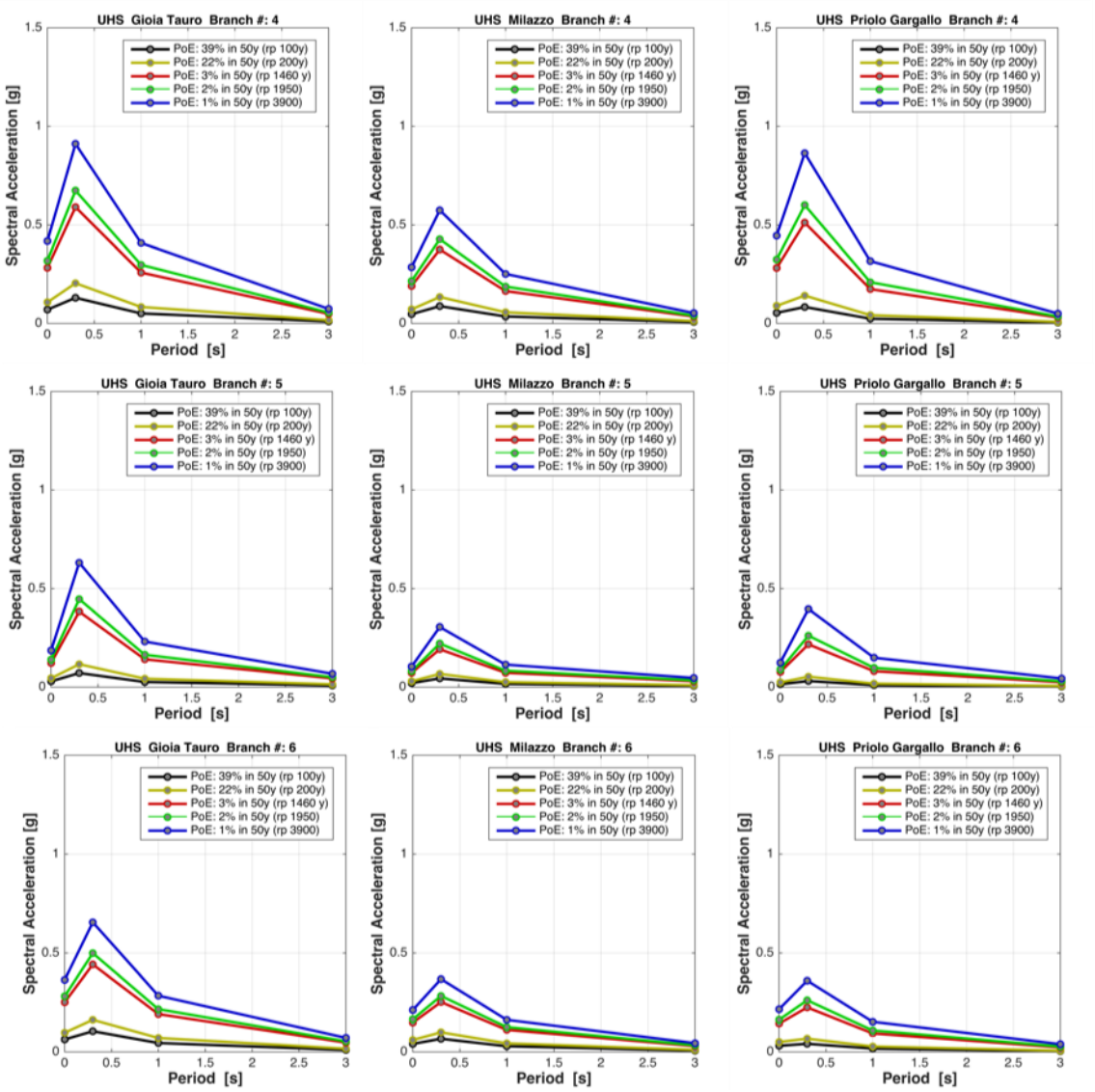
UHS Gioia Tauro Branch #: 4
UHS Milazzo Branch #: 4
UHS Priolo Gargallo Branch #: 4
UHS Gioia Tauro Branch #: 5
UHS Milazzo Branch #: 5
UHS Priolo Gargallo Branch #: 5
UHS Gioia Tauro Branch #: 6
UHS Milazzo Branch #: 6
UHS Priolo Gargallo Branch #: 6
PoE: 39% in 50y (rp 100y)
PoE: 22% in 50y (rp 200y)
PoE: 3% in 50y (rp 1460 y)
PoE: 2% in 50y (rp 1950)
PoE: 1% in 50y (rp 3900)
Spectral Acceleration [g]
Period [s]

Figure B2

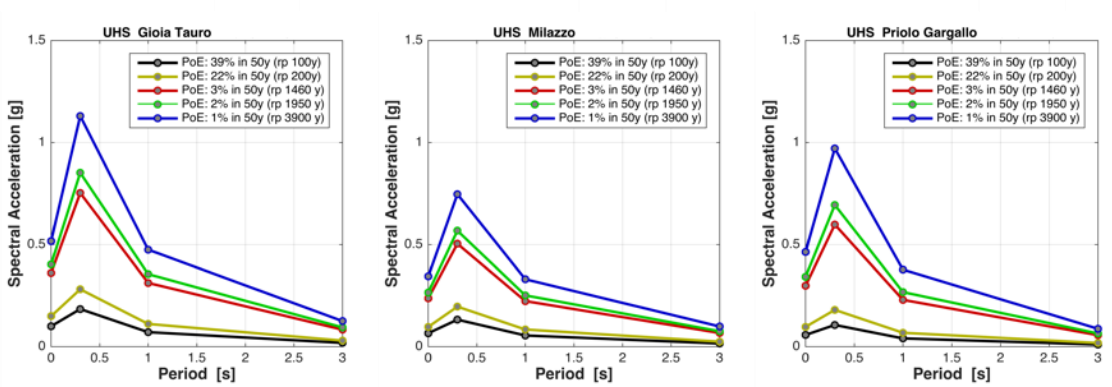

Figure B3

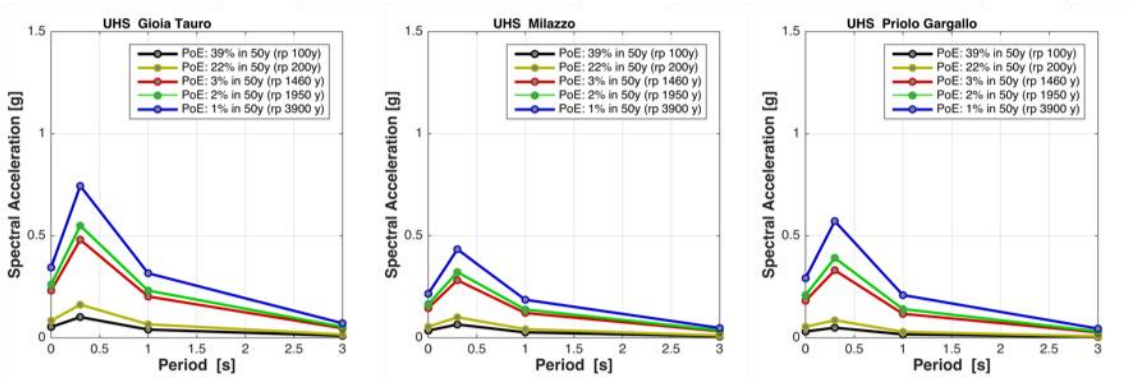

Figure B4

Appendix C

Hazard maps produced for Southern Calabria and Sicily correspondent to each branch of the HYPSTHER project are reported in the following (Figure C1 to Figure C6). The hazard maps for the two branches related to the two seismogenic zonations (Figure C7 for SHARE and Figure C8 for A1MPS16, respectively) are also reported. The hazard is calculated for four intensity measures (PGA, SA at 0.3, 1, and 3 s) and for four return periods (100, 201, 1460, 1950 and 3900 yrs).

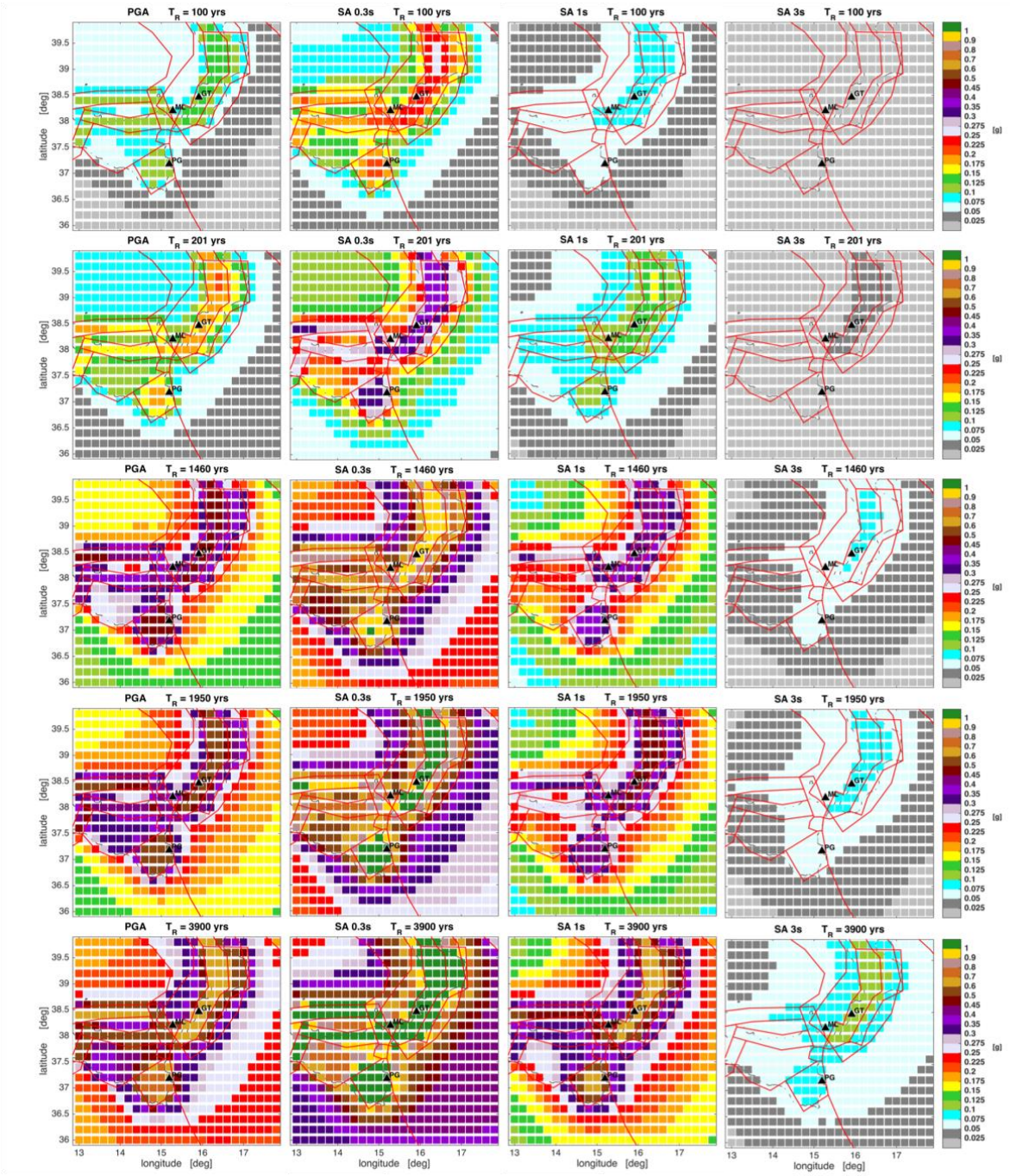
PGA T_R = 100 yrs
SA 0.3s T_R = 100 yrs
SA 1s T_R = 100 yrs
SA 3s T_R = 100 yrs
PGA T_R = 201 yrs
SA 0.3s T_R = 201 yrs
SA 1s T_R = 201 yrs
SA 3s T_R = 201 yrs
PGA T_R = 1460 yrs
SA 0.3s T_R = 1460 yrs
SA 1s T_R = 1460 yrs
SA 3s T_R = 1460 yrs
PGA T_R = 1950 yrs
SA 0.3s T_R = 1950 yrs
SA 1s T_R = 1950 yrs
SA 3s T_R = 1950 yrs
PGA T_R = 3900 yrs
SA 0.3s T_R = 3900 yrs
SA 1s T_R = 3900 yrs
SA 3s T_R = 3900 yrs
latitude [deg]
longitude [deg]
[g]
MC
GT
PG
AM

Figure C1

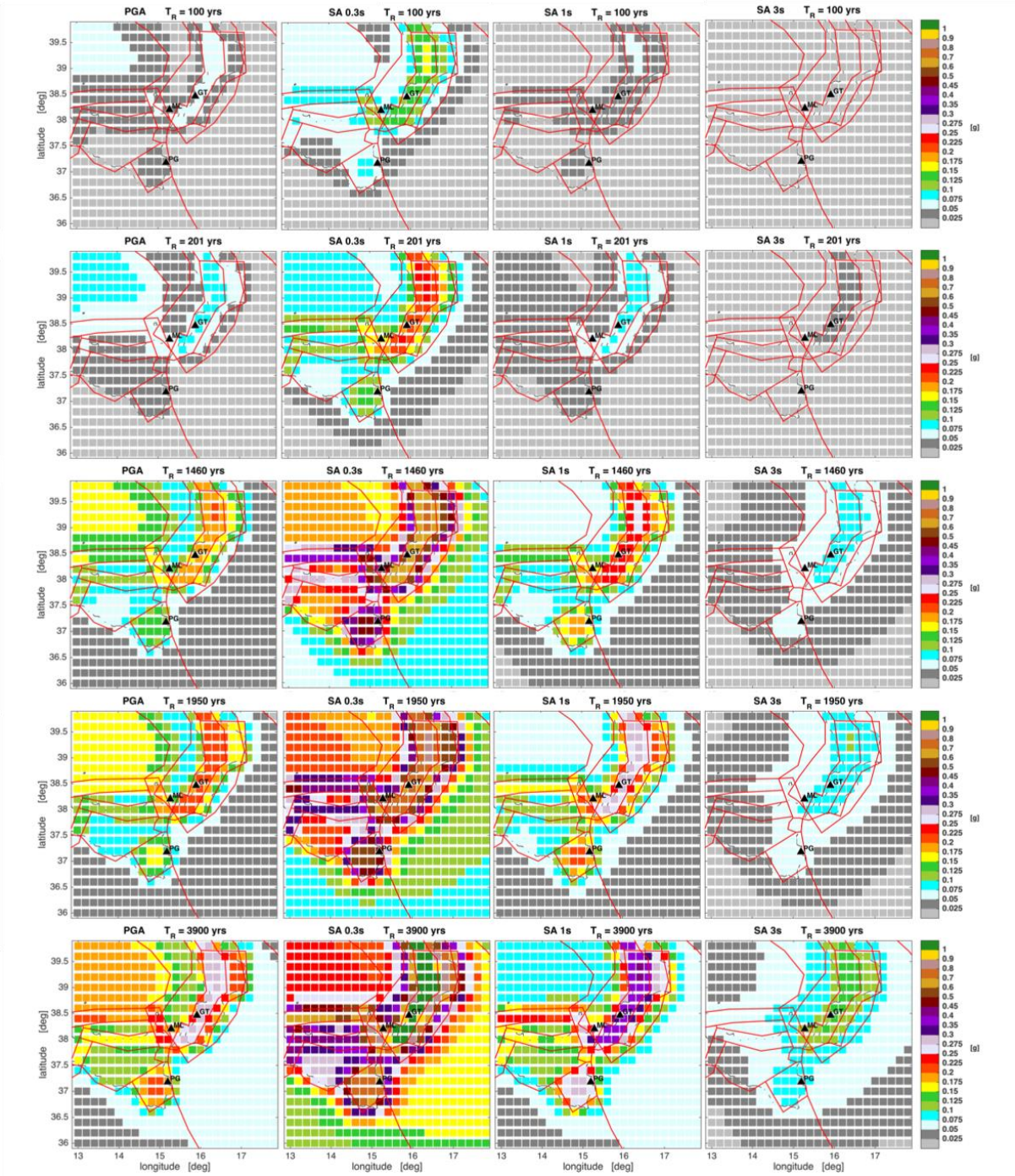
PGA T_R = 100 yrs
SA 0.3s T_R = 100 yrs
SA 1s T_R = 100 yrs
SA 3s T_R = 100 yrs
PGA T_R = 201 yrs
SA 0.3s T_R = 201 yrs
SA 1s T_R = 201 yrs
SA 3s T_R = 201 yrs
PGA T_R = 1460 yrs
SA 0.3s T_R = 1460 yrs
SA 1s T_R = 1460 yrs
SA 3s T_R = 1460 yrs
PGA T_R = 1950 yrs
SA 0.3s T_R = 1950 yrs
SA 1s T_R = 1950 yrs
SA 3s T_R = 1950 yrs
PGA T_R = 3900 yrs
SA 0.3s T_R = 3900 yrs
SA 1s T_R = 3900 yrs
SA 3s T_R = 3900 yrs
latitude [deg]
longitude [deg]
[g]
GT
MC
PG

Figure C2

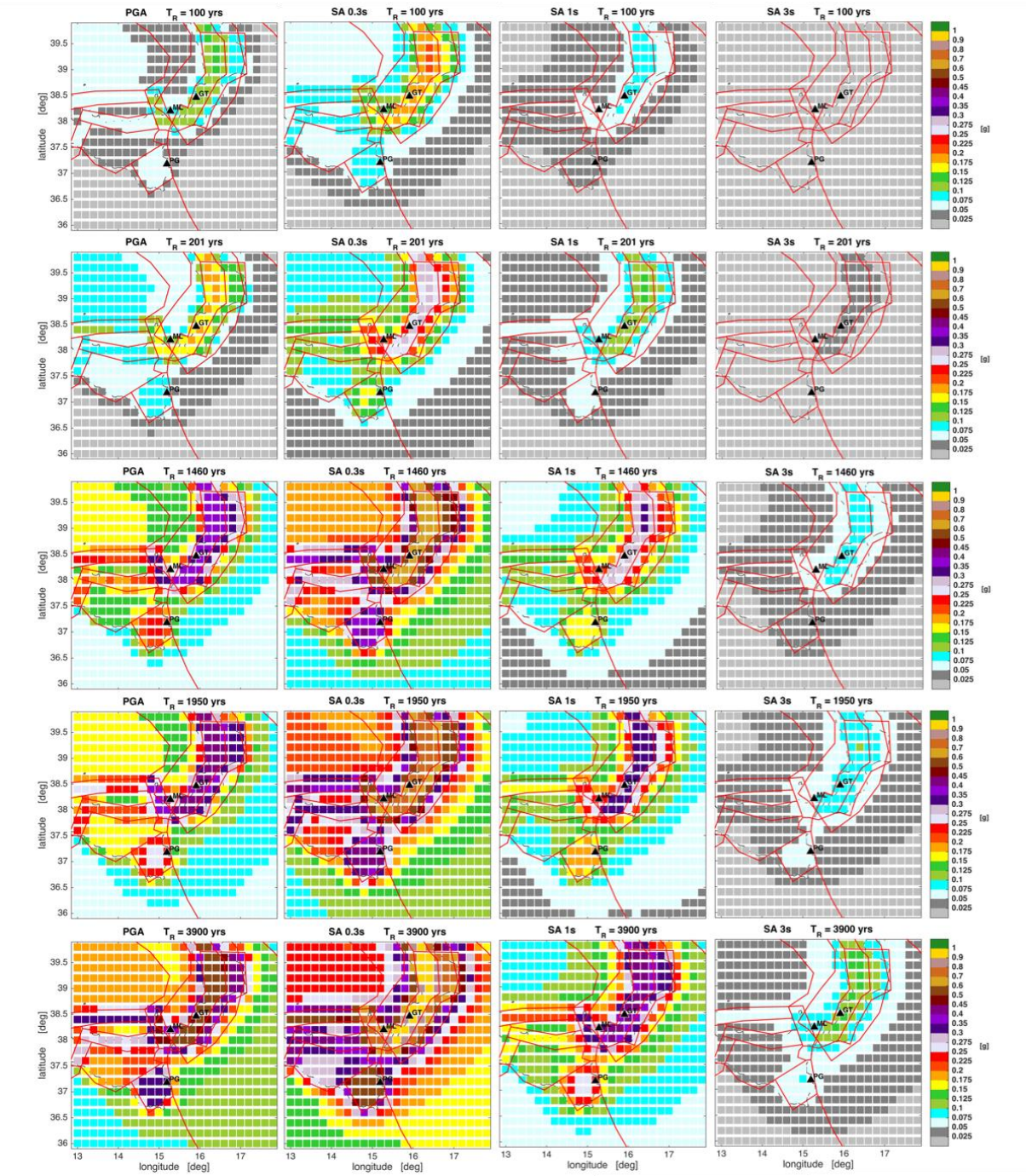
PGA T_R = 100 yrs
SA 0.3s T_R = 100 yrs
SA 1s T_R = 100 yrs
SA 3s T_R = 100 yrs
PGA T_R = 201 yrs
SA 0.3s T_R = 201 yrs
SA 1s T_R = 201 yrs
SA 3s T_R = 201 yrs
PGA T_R = 1460 yrs
SA 0.3s T_R = 1460 yrs
SA 1s T_R = 1460 yrs
SA 3s T_R = 1460 yrs
PGA T_R = 1950 yrs
SA 0.3s T_R = 1950 yrs
SA 1s T_R = 1950 yrs
SA 3s T_R = 1950 yrs
PGA T_R = 3900 yrs
SA 0.3s T_R = 3900 yrs
SA 1s T_R = 3900 yrs
SA 3s T_R = 3900 yrs
latitude [deg]
longitude [deg]
[g]
GT
MC
PG

Figure C3

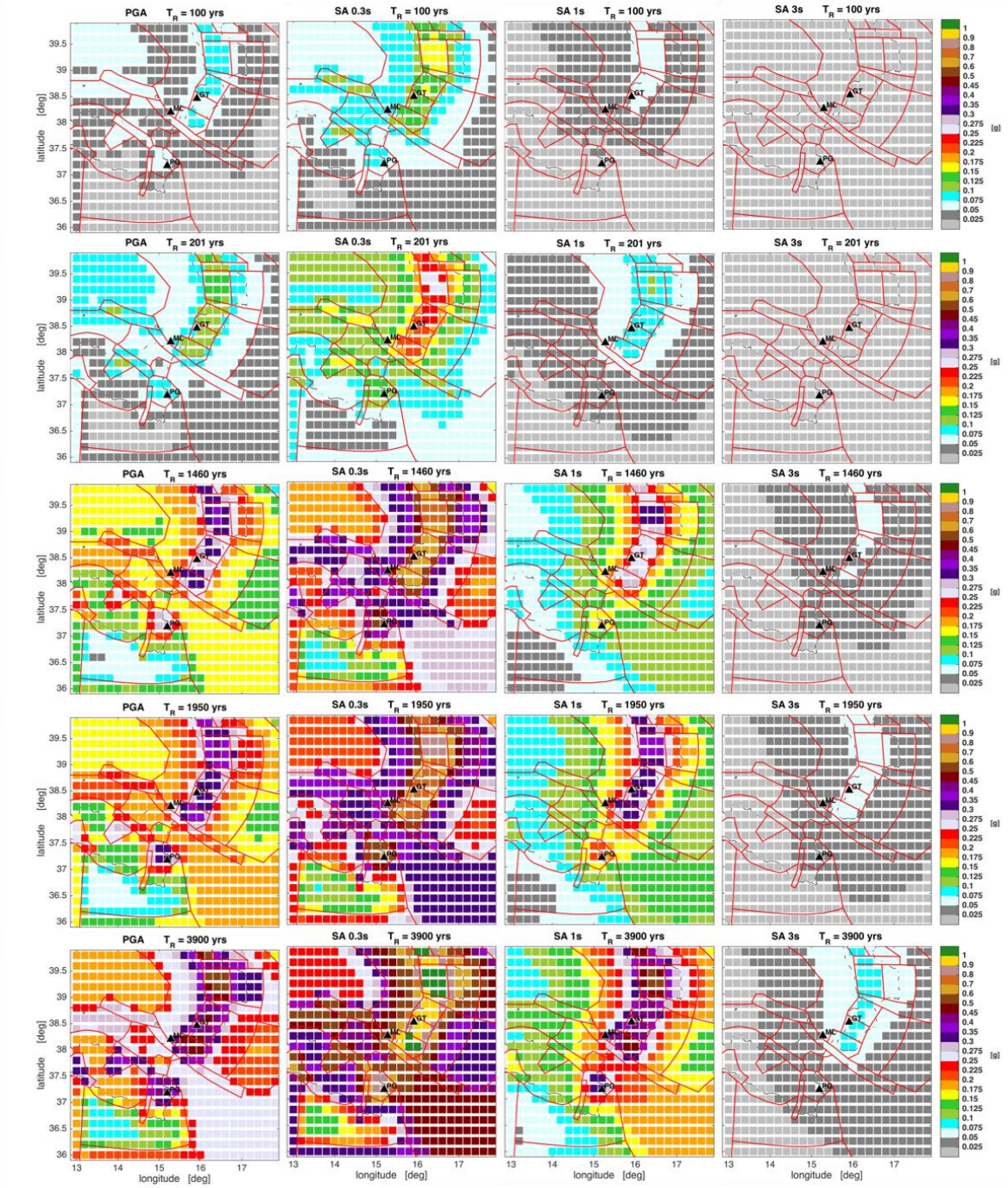
PGA T_R = 100 yrs
SA 0.3s T_R = 100 yrs
SA 1s T_R = 100 yrs
SA 3s T_R = 100 yrs
PGA T_R = 201 yrs
SA 0.3s T_R = 201 yrs
SA 1s T_R = 201 yrs
SA 3s T_R = 201 yrs
PGA T_R = 1460 yrs
SA 0.3s T_R = 1460 yrs
SA 1s T_R = 1460 yrs
SA 3s T_R = 1460 yrs
PGA T_R = 1950 yrs
SA 0.3s T_R = 1950 yrs
SA 1s T_R = 1950 yrs
SA 3s T_R = 1950 yrs
PGA T_R = 3900 yrs
SA 0.3s T_R = 3900 yrs
SA 1s T_R = 3900 yrs
SA 3s T_R = 3900 yrs
latitude [deg]
longitude [deg]
[g]
GT
WC
PG

Figure C4

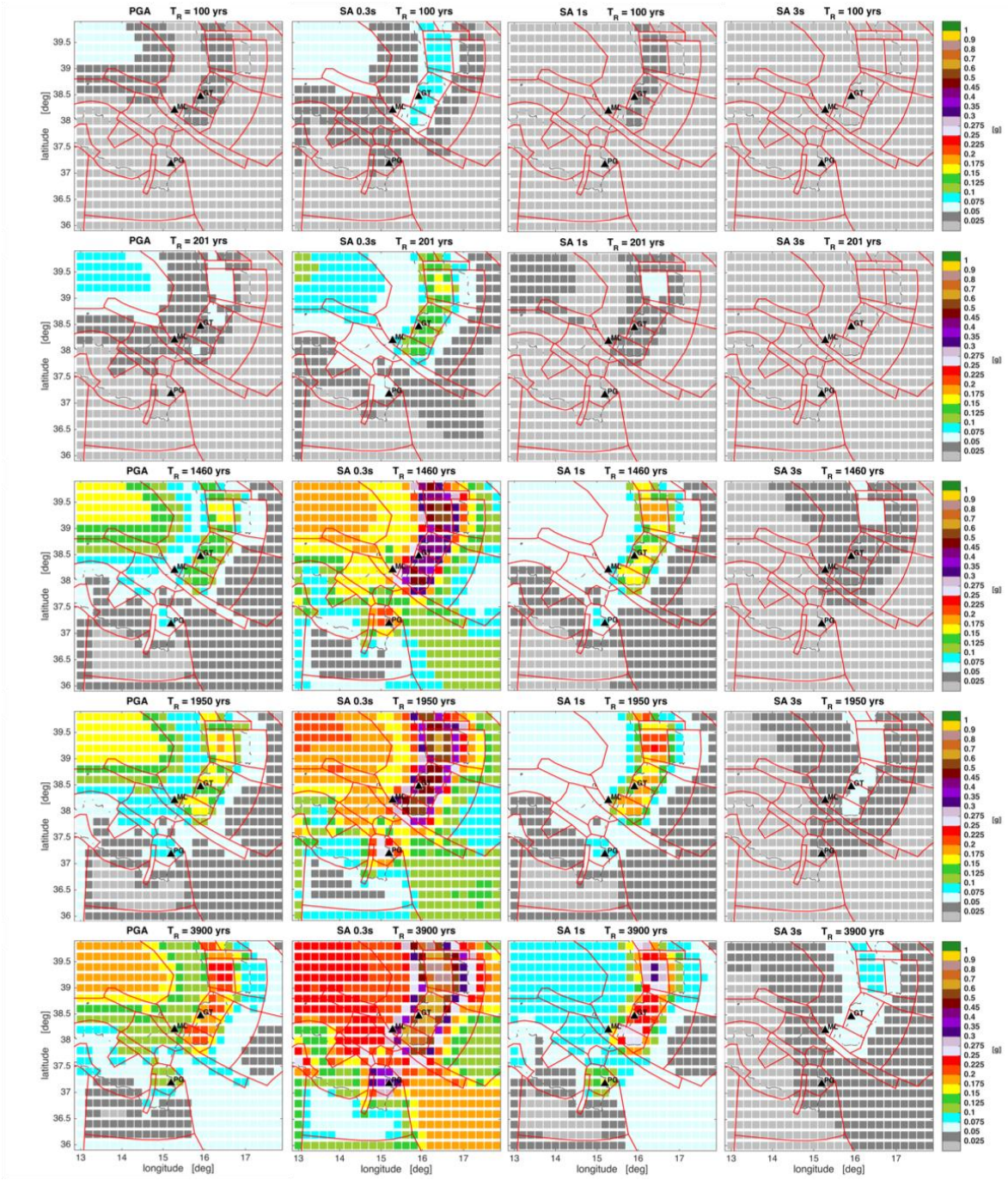
PGA T_R = 100 yrs
SA 0.3s T_R = 100 yrs
SA 1s T_R = 100 yrs
SA 3s T_R = 100 yrs
PGA T_R = 201 yrs
SA 0.3s T_R = 201 yrs
SA 1s T_R = 201 yrs
SA 3s T_R = 201 yrs
PGA T_R = 1460 yrs
SA 0.3s T_R = 1460 yrs
SA 1s T_R = 1460 yrs
SA 3s T_R = 1460 yrs
PGA T_R = 1950 yrs
SA 0.3s T_R = 1950 yrs
SA 1s T_R = 1950 yrs
SA 3s T_R = 1950 yrs
PGA T_R = 3900 yrs
SA 0.3s T_R = 3900 yrs
SA 1s T_R = 3900 yrs
SA 3s T_R = 3900 yrs
latitude [deg]
longitude [deg]
[g]
PG
WC
GT

Figure C5

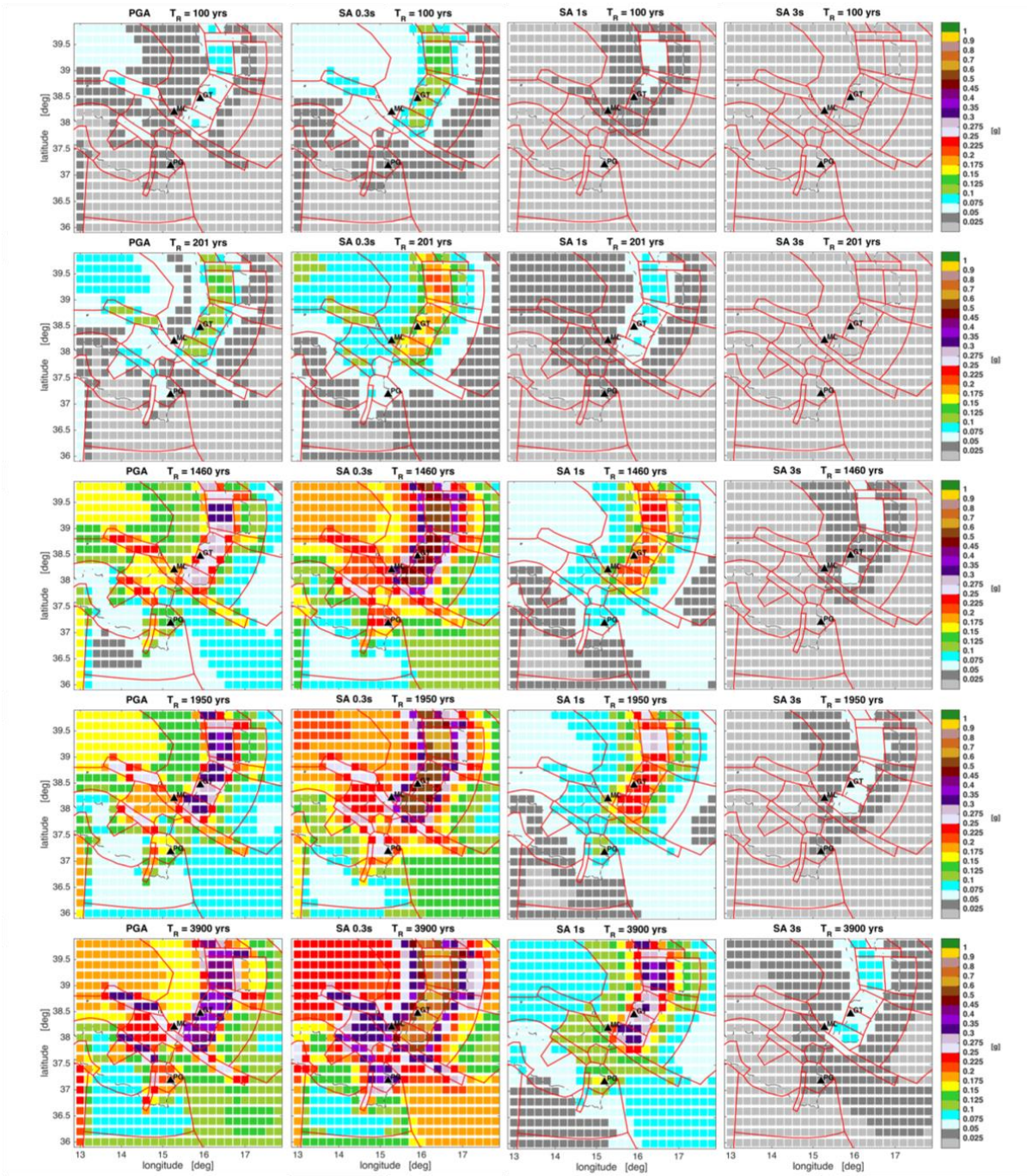
PGA T_R = 100 yrs
SA 0.3s T_R = 100 yrs
SA 1s T_R = 100 yrs
SA 3s T_R = 100 yrs
PGA T_R = 201 yrs
SA 0.3s T_R = 201 yrs
SA 1s T_R = 201 yrs
SA 3s T_R = 201 yrs
PGA T_R = 1460 yrs
SA 0.3s T_R = 1460 yrs
SA 1s T_R = 1460 yrs
SA 3s T_R = 1460 yrs
PGA T_R = 1950 yrs
SA 0.3s T_R = 1950 yrs
SA 1s T_R = 1950 yrs
SA 3s T_R = 1950 yrs
PGA T_R = 3900 yrs
SA 0.3s T_R = 3900 yrs
SA 1s T_R = 3900 yrs
SA 3s T_R = 3900 yrs
latitude [deg]
longitude [deg]
[g]
AVC
AGT
PGS

Figure C6

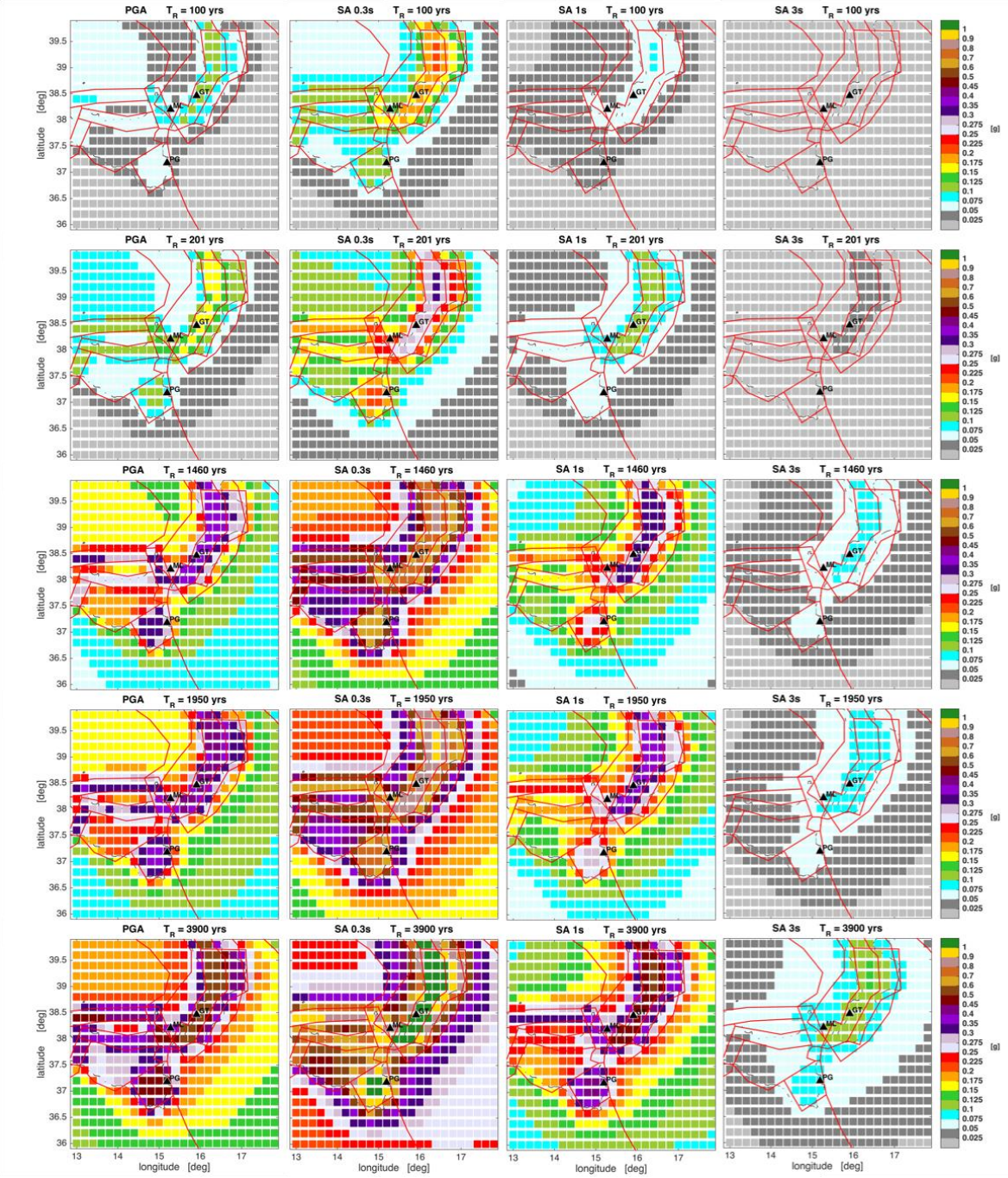
PGA T_R = 100 yrs
SA 0.3s T_R = 100 yrs
SA 1s T_R = 100 yrs
SA 3s T_R = 100 yrs
PGA T_R = 201 yrs
SA 0.3s T_R = 201 yrs
SA 1s T_R = 201 yrs
SA 3s T_R = 201 yrs
PGA T_R = 1460 yrs
SA 0.3s T_R = 1460 yrs
SA 1s T_R = 1460 yrs
SA 3s T_R = 1460 yrs
PGA T_R = 1950 yrs
SA 0.3s T_R = 1950 yrs
SA 1s T_R = 1950 yrs
SA 3s T_R = 1950 yrs
PGA T_R = 3900 yrs
SA 0.3s T_R = 3900 yrs
SA 1s T_R = 3900 yrs
SA 3s T_R = 3900 yrs
latitude [deg]
longitude [deg]
[g]
GT
MC
PG

Figure C7

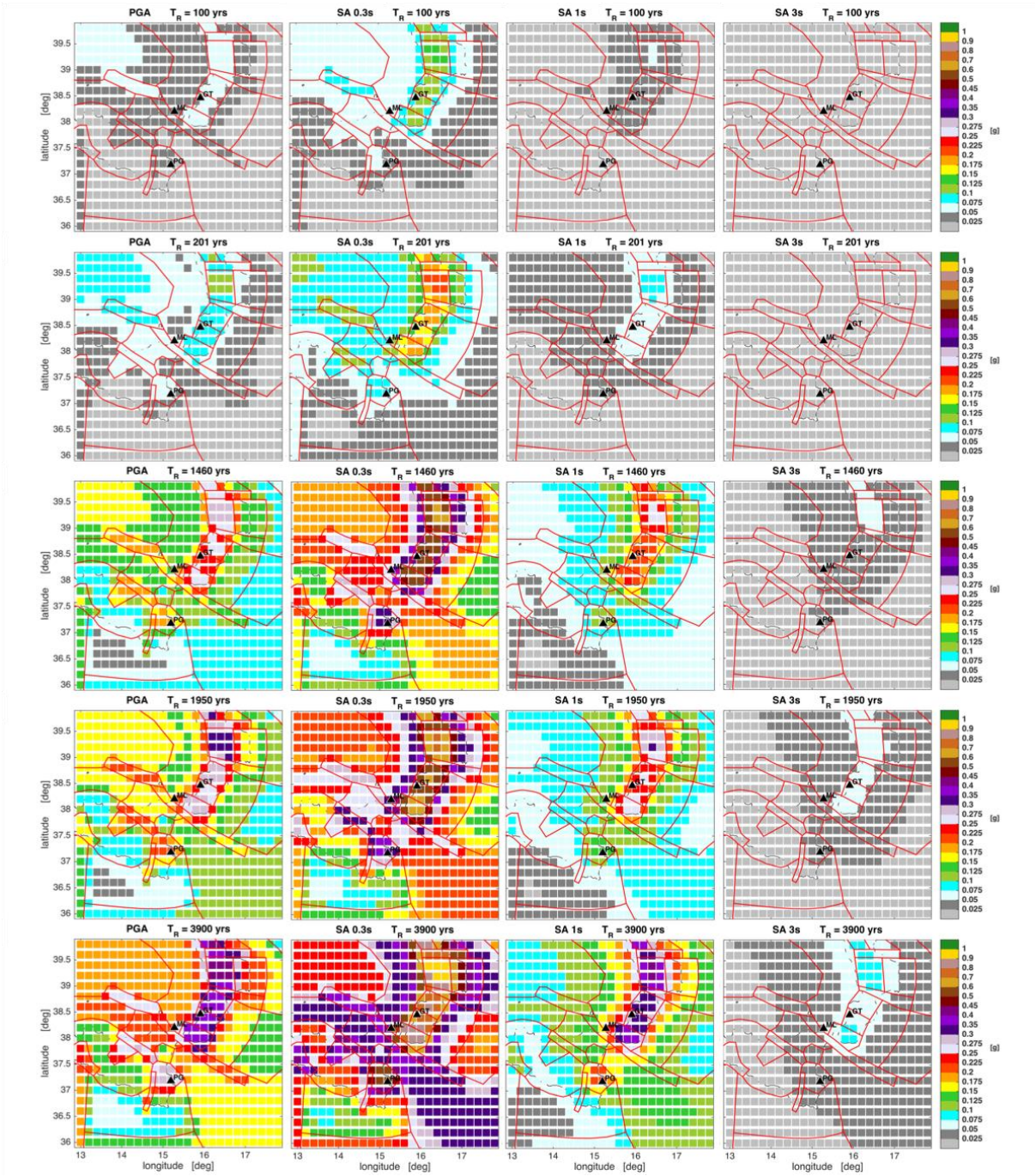
PGA T_R = 100 yrs
SA 0.3s T_R = 100 yrs
SA 1s T_R = 100 yrs
SA 3s T_R = 100 yrs
PGA T_R = 201 yrs
SA 0.3s T_R = 201 yrs
SA 1s T_R = 201 yrs
SA 3s T_R = 201 yrs
PGA T_R = 1460 yrs
SA 0.3s T_R = 1460 yrs
SA 1s T_R = 1460 yrs
SA 3s T_R = 1460 yrs
PGA T_R = 1950 yrs
SA 0.3s T_R = 1950 yrs
SA 1s T_R = 1950 yrs
SA 3s T_R = 1950 yrs
PGA T_R = 3900 yrs
SA 0.3s T_R = 3900 yrs
SA 1s T_R = 3900 yrs
SA 3s T_R = 3900 yrs
latitude [deg]
longitude [deg]
[g]
GT
AW
PG

Figure C8

Appendix D

Exceedance probability curves (50 yrs) related to the SHARE (Figure D1) and to the A1MPS16 (Figure D2). The hazard is calculated for the three test sites (Gioia Tauro, Milazzo, and Priolo Gargallo) and for four intensity measures (PGA, SA at 0.3, 1, and 3 s).

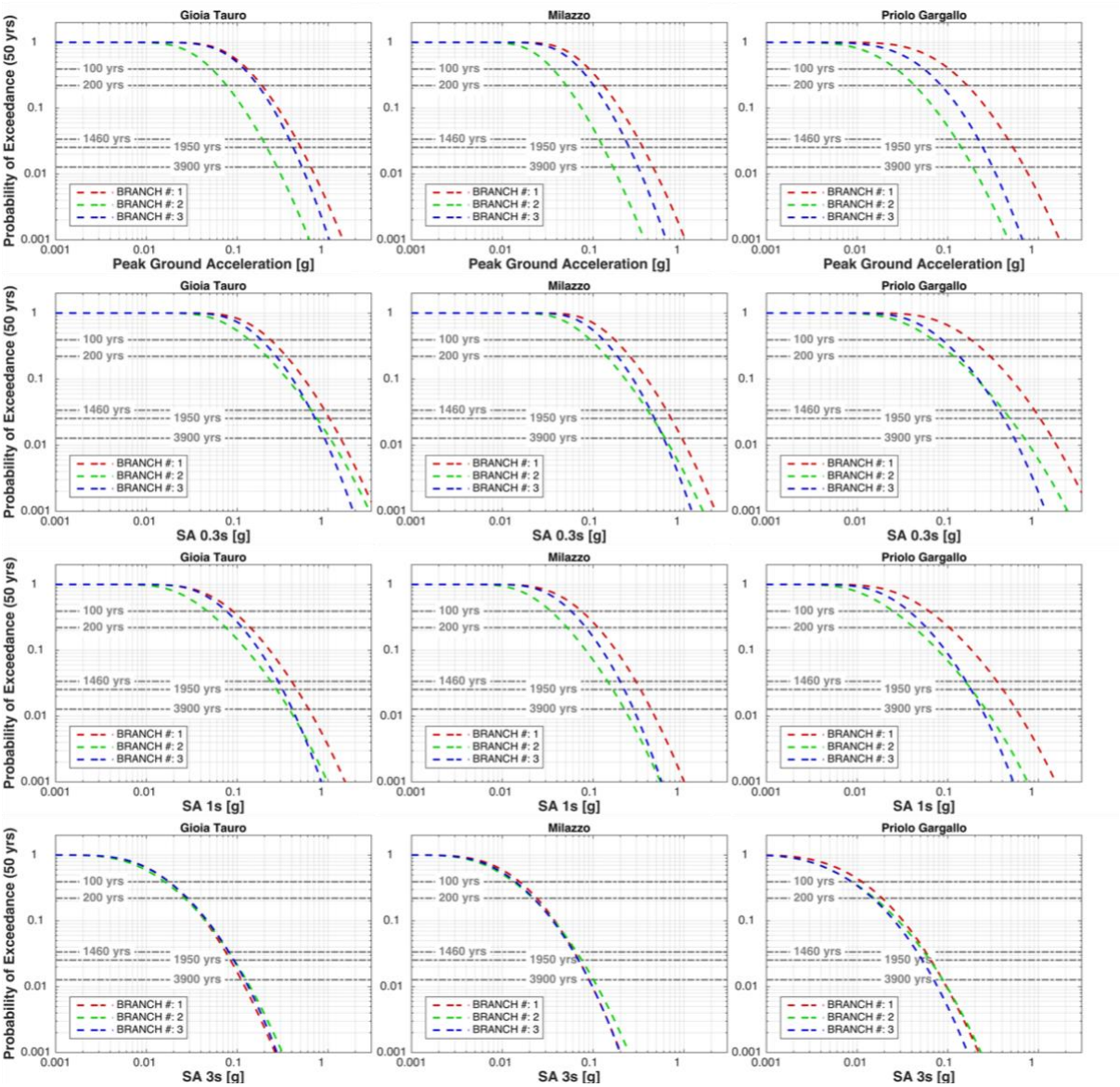
Gioia Tauro
Milazzo
Priolo Gargallo
Probability of Exceedance (50 yrs)
100 yrs
200 yrs
1460 yrs
1950 yrs
3900 yrs
BRANCH #: 1
BRANCH #: 2
BRANCH #: 3
Peak Ground Acceleration [g]
SA 0.3s [g]
SA 1s [g]
SA 3s [g]

Figure D1

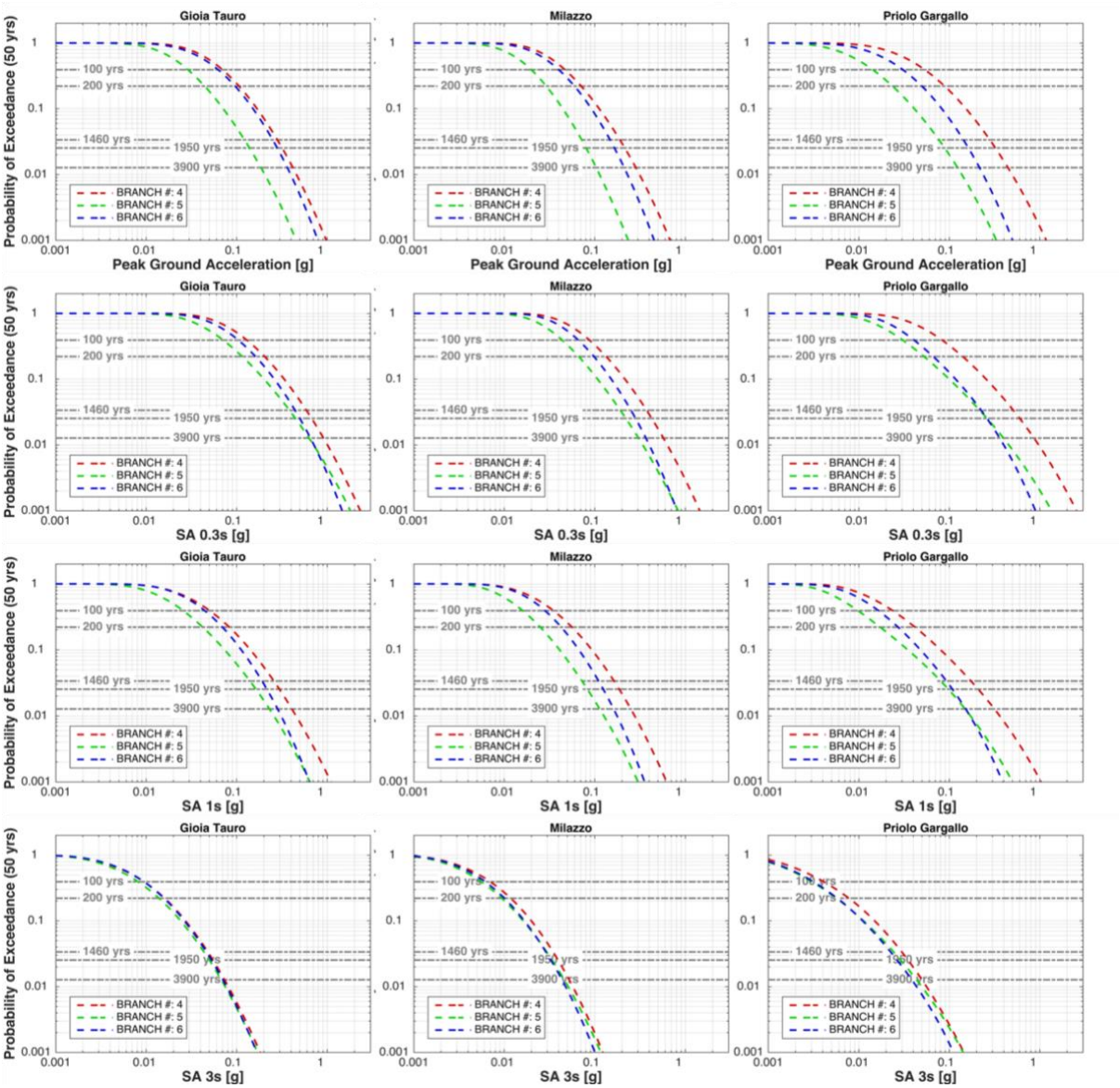
Gioia Tauro
Milazzo
Priolo Gargallo
Probability of Exceedance (50 yrs)
100 yrs
200 yrs
1460 yrs
1950 yrs
3900 yrs
BRANCH #: 4
BRANCH #: 5
BRANCH #: 6
Peak Ground Acceleration [g]
SA 0.3s [g]
SA 1s [g]
SA 3s [g]

Figure D2

Appendix E

Uniform Hazard Spectra (UHS) in 50 yrs correspondent to SHARE (Figure E1) and A1MPS16 (Figure E2). The hazard is calculated for the three test sites (Gioia Tauro, Milazzo and Priolo Gargallo) and for four intensity measures (PGA, SA at 0.3, 1, and 3 s).

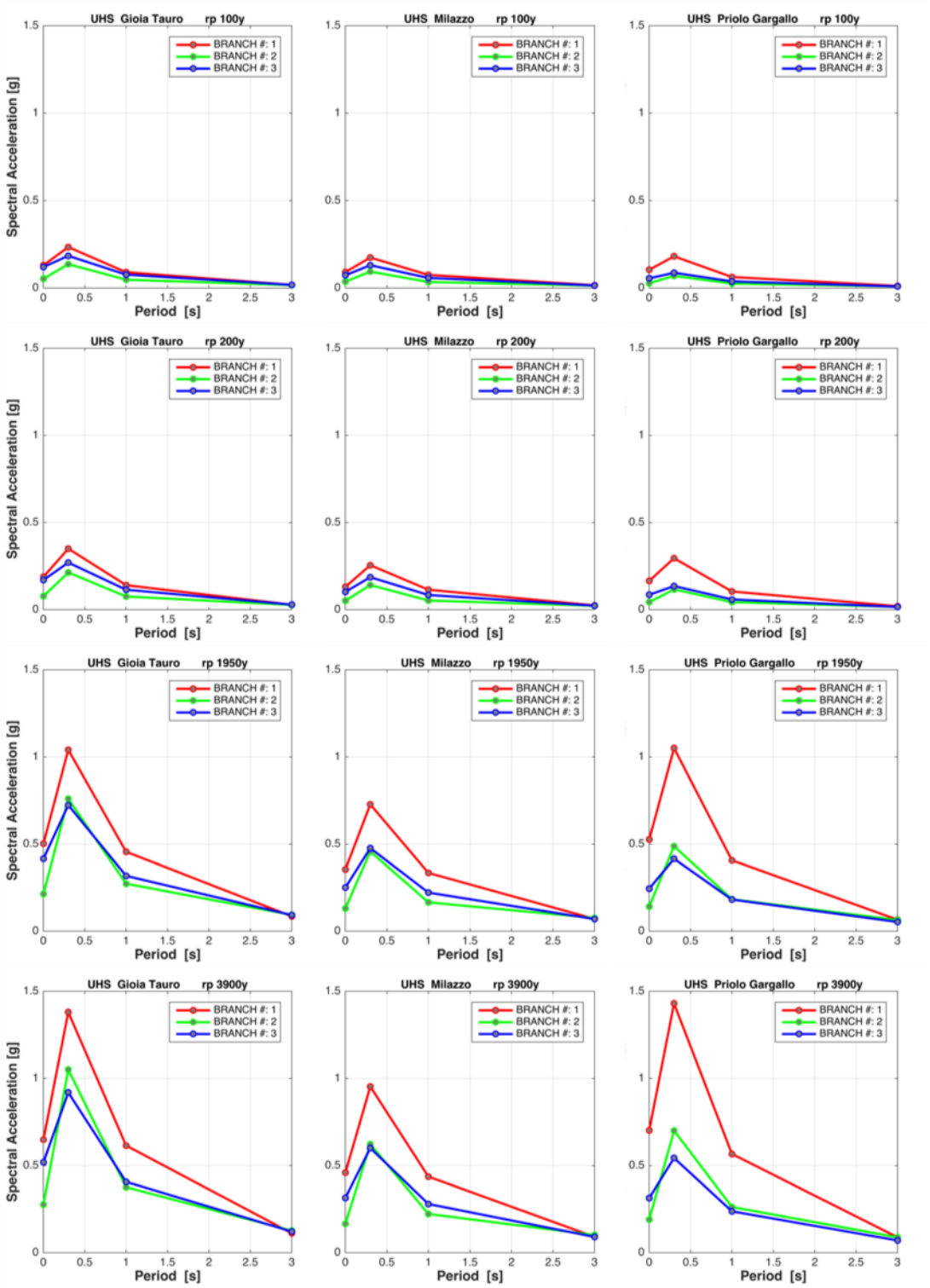
UHS Gioia Tauro rp 100y
UHS Milazzo rp 100y
UHS Priolo Gargallo rp 100y
UHS Gioia Tauro rp 200y
UHS Milazzo rp 200y
UHS Priolo Gargallo rp 200y
UHS Gioia Tauro rp 1950y
UHS Milazzo rp 1950y
UHS Priolo Gargallo rp 1950y
UHS Gioia Tauro rp 3900y
UHS Milazzo rp 3900y
UHS Priolo Gargallo rp 3900y
BRANCH #: 1
BRANCH #: 2
BRANCH #: 3
Spectral Acceleration [g]
Period [s]

Figure E1

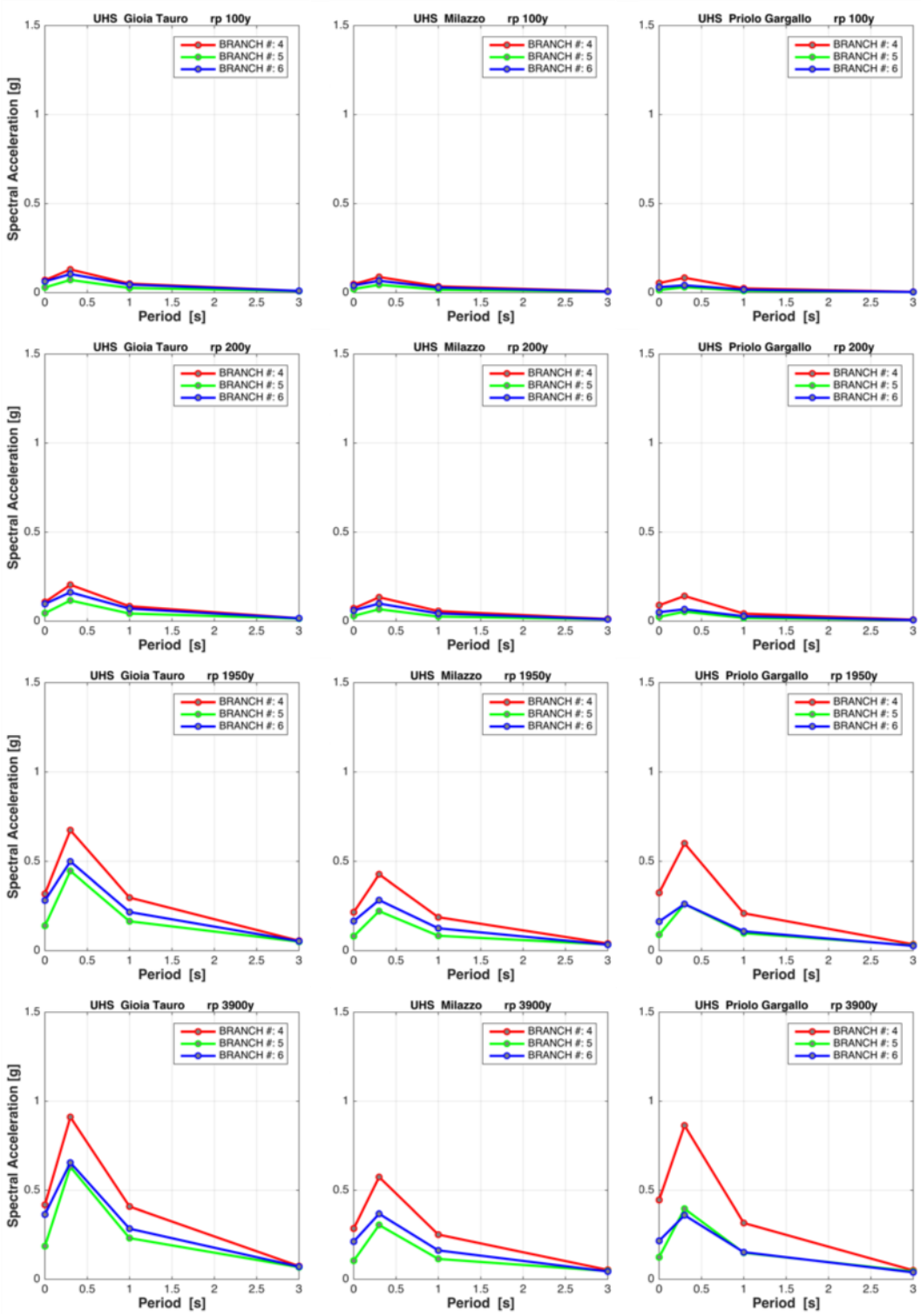
UHS Gioia Tauro rp 100y
UHS Milazzo rp 100y
UHS Priolo Gargallo rp 100y
UHS Gioia Tauro rp 200y
UHS Milazzo rp 200y
UHS Priolo Gargallo rp 200y
UHS Gioia Tauro rp 1950y
UHS Milazzo rp 1950y
UHS Priolo Gargallo rp 1950y
UHS Gioia Tauro rp 3900y
UHS Milazzo rp 3900y
UHS Priolo Gargallo rp 3900y
BRANCH #: 4
BRANCH #: 5
BRANCH #: 6
Spectral Acceleration [g]
Period [s]

Figure E2

Appendix F

Magnitude-Distance distribution resulting from disaggregation of PGA by using A1MPS16 seismic zonation and SI17hyb attenuation model. The disaggregation is calculated for the three test sites (Gioia Tauro, Milazzo and Priolo Gargallo) and corresponds to the Serviceability Limit State for damage control (SLD, upper panel in Figure F1) and the Ultimate Limit State for collapse prevention (SLC, bottom panel in Figure F1).

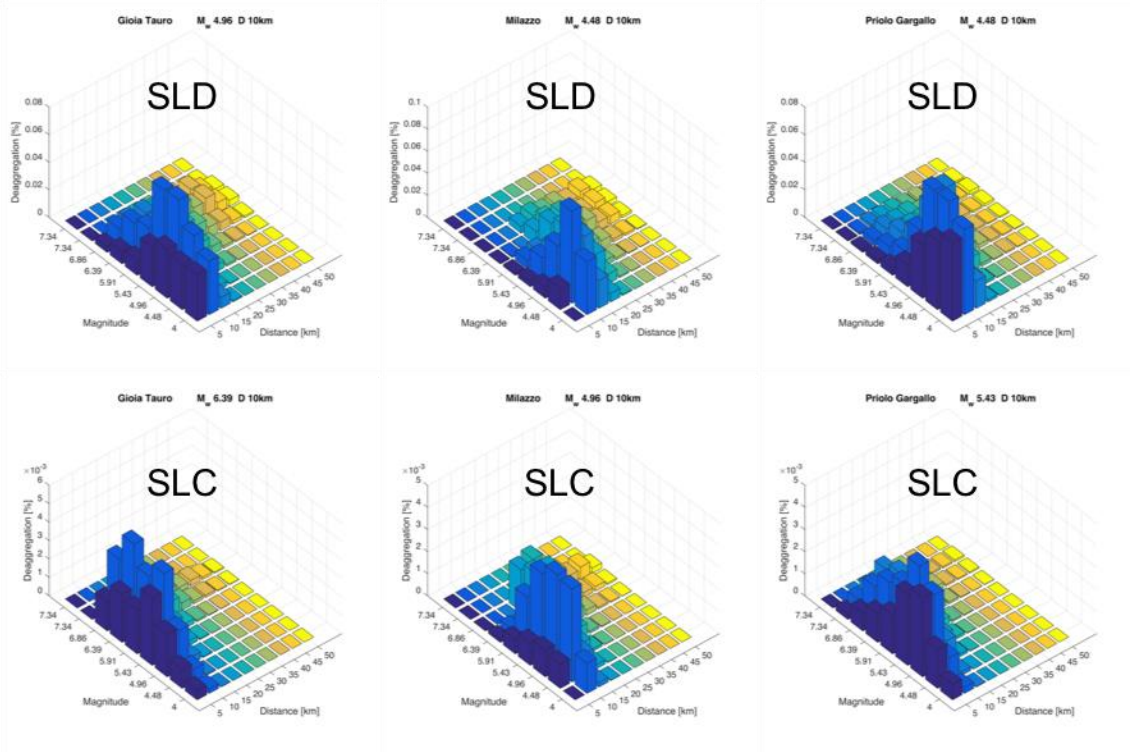
Gioia Tauro M_w 4.96 D 10km
SLD
Milazzo M_w 4.48 D 10km
SLD
Priolo Gargallo M_w 4.48 D 10km
SLD
Gioia Tauro M_w 6.39 D 10km
SLC
Milazzo M_w 4.96 D 10km
SLC
Priolo Gargallo M_w 5.43 D 10km
SLC
Deaggregation [%]
Magnitude
Distance [km]

Figure F1

Disclaimer

Any result included in the document is based on the available scientific knowledge and is devoted to qualified users. Every risk due to the improper use of data or the use of inaccurate information is assumed by the user.

Creative Commons

Citation

This Deliverable must be cited as follow: "**Santulin M., D'Amico M., Lanzano G. (2018). Seismic Hazard Assessment.** Istituto Nazionale di Geofisica e Vulcanologia, HYPSTHER project, http://hypsther.mi.ingv.it/ - doi: 10.5281/zenodo.1187030".